Telomerase related molecular subtype and risk model reveal immune activity and evaluate prognosis and immunotherapy response in prostate cancer

Dongze Liu[1†], Zheng Qin[2†], Bocun Yi[1†], Hongbo Xie[1†], Yunan Liang[1†], Liang Zhu[1], Kuo Yang[1], Yong Xu[1*] and Hongtuan Zhang[1*]

Abstract

Background Prostate cancer ranks among the six most lethal malignancies worldwide. Telomerase, a reverse transcriptase enzyme, plays a pivotal role in extending cellular telomeres and is intimately associated with cell proliferation and division. However, the interconnection between prostate cancer and telomerase-related genes (TEASEs) remains unclear.

Methods Somatic mutations and copy number alterations of TEASEs were comprehensively analyzed. Subsequently, the transcripts of prostate cancer patients in TCGA and GEO databases were integrated to delineate new molecular subtypes. Followed by constructing a risk model containing nine characteristic genes through Lasso regression and Cox prognostic analysis among different subtypes. Various aspects including prognosis, tumor microenvironment (TME), landscape of immunity, tumor mutational burden (TMB), stem cell correlation, and median inhibitory concentration amongst different risk groups were compared. Finally, the expression, prognosis, and malignant biological behavior of ZW10 interactor (ZWINT) in vitro was explored.

Results TEASEs exhibited a notably high mutation frequency. Three distinct molecular subtypes and two gene subclusters based on TEASEs were delineated, displaying significant associations with prognosis, immune function regulation, and clinical characteristics. Low-risk patients demonstrated superior prognosis and better response to immunotherapy. Conversely, high-risk patients exhibited higher TMB and stronger stem cell correlations. It was also found that the patients' sensitivity to chemotherapy agents was impacted by the risk score. Finally, ZWINT's potential as a novel diagnostic and prognostic biomarker for prostate cancer was validated.

[†]Dongze Liu, Zheng Qin, Bocun Yi, Hongbo Xie and Yunan Liang contributed identically and share first authorship in our research work

*Correspondence:
Yong Xu
xymnwk@163.com
Hongtuan Zhang
zhtlml@tmu.edu.cn

Full list of author information is available at the end of the article

Conclusions TEASEs play a pivotal role in modulating immune regulation and immunotherapeutic responses, thereby significantly impacting the diagnosis, prognosis, and treatment strategies for affected patients.

Keywords Telomerase, Prostate cancer, Molecular subtype, Risk model, Immunotherapy, ZWINT

Introduction

Prostate cancer is one of the top six leading malignancies, exhibiting a mortality rate of 3.8 per 100,000 people in Asian countries and resulting in 85,200 deaths per year in Europe [1, 2]. Surgery and radiotherapy serve as curative modalities for prostate cancer. However, side effects, such as sexual dysfunction and urinary symptoms, often come with these treatments and are incurable [3, 4]. Immunotherapy has changed the treatment paradigm for multiple cancer types but its definitive role in unselected prostate cancer patients remains to be explored [5]. Improving prostate cancer risk stratification and finding new biomarkers can benefit the diagnosis and treatment of prostate cancer [3]. Therefore, it is of vital importance to explore novel markers of prostate cancer and construct a characteristic risk model for it.

Telomeres are repetitive DNA sequences located at the chromosome endings and they are responsible for protecting the chromosomes. With an increasing number of cell divisions, the length of telomeres undergoes a gradual shortening process. This process is ceased when DNA damage and cell apoptosis mediated by the P53 signaling pathway are triggered [6]. Telomerase is a ribonucleoprotein complex in eukaryotes, and it adds repeated TTAGGG sequences to telomeres through its internal reverse transcription template to further maintain the stability of the telomere length. Telomerase activity has been observed in abundant tumor tissues, whereas it has not been found in corresponding benign tissues [7]. Therefore, TEASEs may have the potential to serve as a new biomarker and molecular therapeutic target for prostate cancer. In our study, prostate cancer patients were divided into 3 different molecular subgroups, based on their expression of TEASEs. The gene differential expression difference and prognostic correlations across different molecular subgroups were analyzed, and 41 differential and prognostic-related genes were identified. These genes guided the establishment of 2 distinct gene subclusters and telomerase-related risk score models. The attributes of the risk model were elucidated by subsequent assessments, including survival prognostic analysis, clinicopathological correlations, biochemical recurrence analysis, immune characteristics, mutation correlation analysis, cancer stem cell analysis, and sensitivity to chemotherapeutic agents or immunotherapy. Lastly, in vitro and in vivo experimental validations were conducted to confirm the potential of ZWINT as a diagnostic and prognostic marker.

Results

Expression of TEASEs and corresponding prognosis and molecular changes

The workflow of our study was shown in Fig. 1. We first analyzed the mutation frequency of 67 TEASEs in somatic cells from the TCGA PRAD database. Overall, the mutation frequency was relatively high, as 63 of the 495 samples (12.73%) were found to have mutations. The highest mutation frequency was 4% for ATM and 1% for CDKN1B, ZNFX1, ABL1, AKT1, EGF, EGFR, MTOR, NBN, SIN3B, TNKS and XRCC6 (Fig. 2A). In subsequent analysis of somatic copy number alterations, copy number gains and losses were widespread in TEASEs (Fig. 2B), and the specific chromosomal locations of copy number alterations were shown in Fig. 2C. Next, we analyzed the differential expression of TEASEs in tumor and normal samples from TCGA database. Interestingly, the expression of 16 genes were upregulated and 24 genes were downregulated in prostate cancer compared to normal tissue (Fig. 2D). In summary, the molecular changes of TEASEs may play a significant role in modulating the development of prostate cancer. To understand the clinical prognostic significance of TEASEs, we performed KM analysis and uniCox analysis on 500 prostate cancer samples collected from TCGA and 281 prostate cancer samples collected from GEO (GSE16560). The findings revealed that 28 TEASEs displayed association with the overall survival of prostate cancer patients in KM analysis (Table 1). The relationship network of 28 TEASEs and their potential prognostic significance were graphically presented (Fig. 2E).

Establishment and analysis of subgroups related to TEASEs

We performed consensus clustering analysis on the TEASEs transcript data of TCGA PRAD and GSE16560. In the co-clustering analysis, the data was categorized into three clusters, with the darkest color within each cluster indicating the smallest variation within that specific cluster, and the lightest color between clusters representing the most significant differences between them (Fig. 3A). Furthermore, the Cumulative Distribution Function (CDF) curve exhibited the most pronounced change when k=3, compelling us to divide the samples into three clusters (Fig. 3B). Specifically, Clusters 1, 2, and 3 corresponded to clusters A (294 samples), B (371 samples), and C (113 samples), respectively. In the subsequent survival analysis, cluster C presented the best survival prognosis while cluster A presented the poorest survival prognosis (Fig. 3C). Specific expression
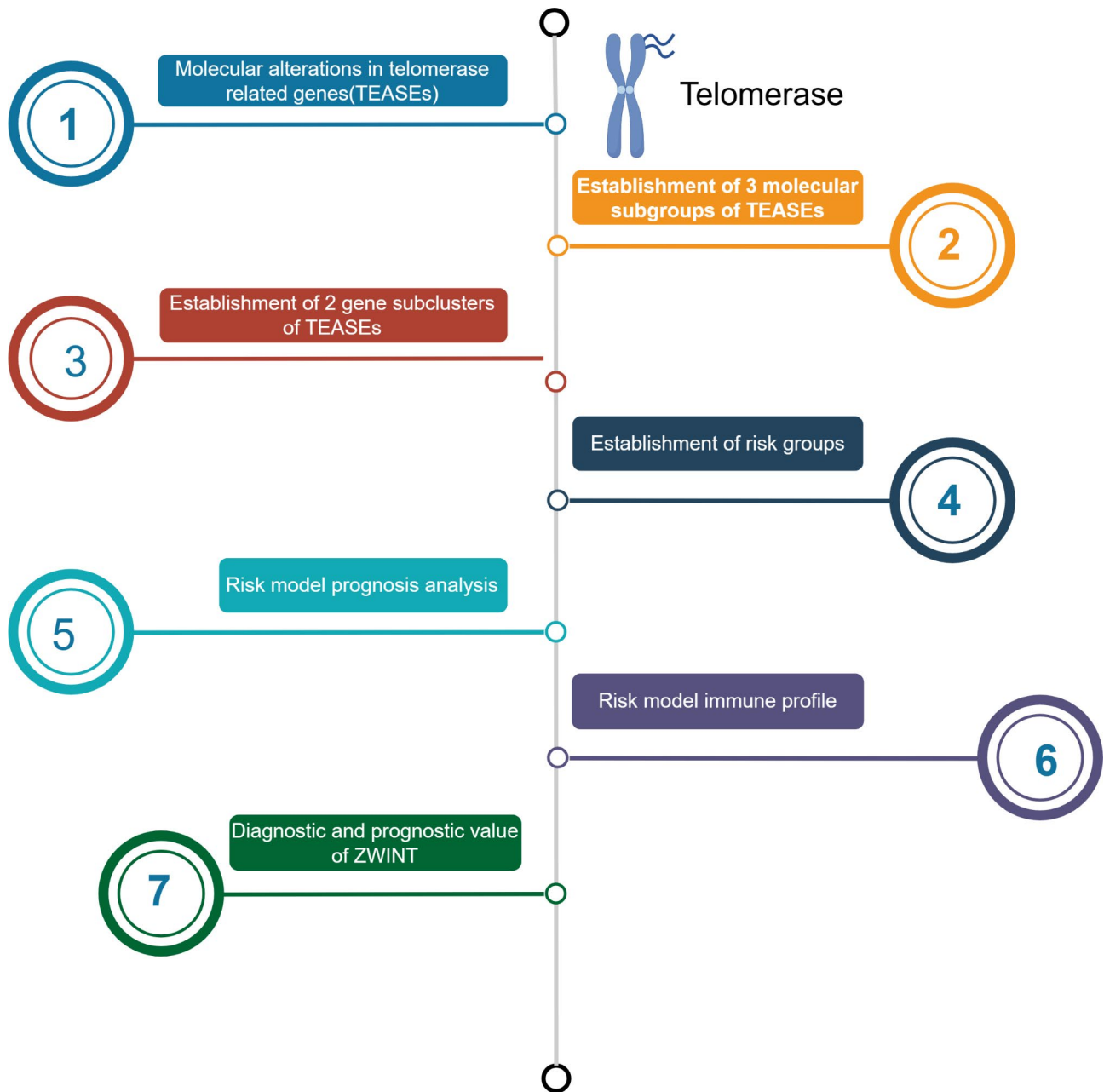
Fig. 1 Workflow

distribution of TEASEs in different subtypes, N/T stage, gleason score, and age was shown in a heatmap (Fig. 3D). The twenty most statistically significant pathways between subtypes were also identified using GSVA analysis (Fig. 3E-G). To preliminarily reveal the connection between different subtypes and tumor immune microenvironments (IME), the ssGSEA method was utilized to evaluate the infiltration of various immune cells in different subtypes. The findings showed that infiltrating abundance of 21 types of immune cells had notable variations in the distribution amongst the three different

subtypes, indicating that different subtypes have different IME characteristics (Fig. 3H).

Intersection between different subtypes and analysis of corresponding biological functions

The principal component analysis suggested that the three different subtypes could be well distinguished according to the gene expression of TEASES (Fig. 4A). The pairwise difference analysis was subsequently performed on the 3 subtypes (A-B, A-C, B-C) and obtained 321differentially expressed genes (DEGs) with common intersection (Fig. 4B). In the GO and KEGG analysis of
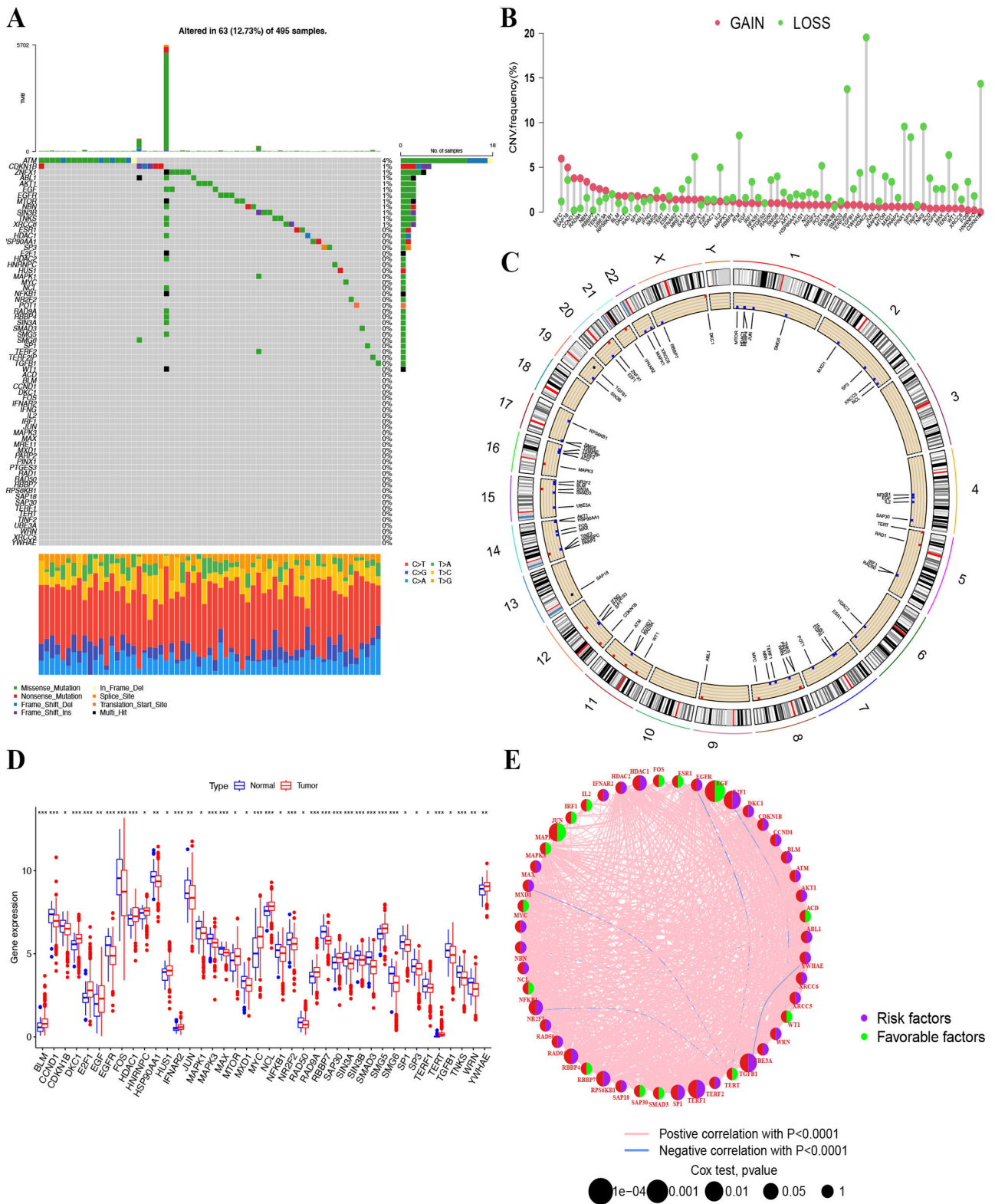
Fig. 2 Molecular changes and differential expression of TEASEs in prostate cancer. (**A**) TEASEs somatic mutation frequency. (**B**) Somatic copy number alterations of TEASEs. (**C**) Chromosomal copy number alteration locations of TEASEs and red or blue represents an increase or decrease in copy number. (**D**) Differential expression of TEASEs between prostate cancer and normal tissue samples. (**E**) TEASEs prognostic network diagram

Table 1 Survival prognostic analysis of TEASEs

id	HR	HR.95 L	HR.95 H	*p*-value
TERF1	1.360332	1.083482	1.707922	2.14E-05
HDAC1	1.325812	1.027642	1.710496	5.95E-05
E2F1	1.258835	1.065307	1.48752	6.15E-05
JUN	0.809933	0.696207	0.942236	0.000192
EGF	0.802419	0.715329	0.900113	0.000647
RPS6KB1	1.525155	1.087122	2.139684	0.000666
MAX	1.527123	0.997088	2.338917	0.003073
TGFB1	1.279442	1.060703	1.543291	0.003967
SP1	1.330168	1.013686	1.745458	0.005813
TERF2	1.159369	0.948595	1.416976	0.006369
RBBP4	1.397369	1.068068	1.828199	0.008171
MAPK3	1.098239	0.877966	1.373777	0.010259
AKT1	1.067908	0.869053	1.312263	0.011244
HDAC2	1.232111	0.953797	1.591637	0.011917
NR2F2	1.330277	1.007734	1.756054	0.012645
XRCC5	1.336247	0.98372	1.815106	0.012888
WRN	1.066494	0.865688	1.313878	0.015635
EGFR	1.107396	0.94407	1.298978	0.018788
RAD9A	1.042127	0.820313	1.323919	0.023731
DKC1	1.306299	0.995686	1.713809	0.026347
ESR1	0.934511	0.797315	1.095315	0.027427
NCL	1.284172	0.948709	1.738256	0.02769
MXD1	0.821199	0.656021	1.027966	0.031465
RAD50	1.075445	0.821886	1.40723	0.033061
NFKB1	0.982402	0.810675	1.190507	0.036731
ABL1	1.042976	0.866716	1.25508	0.040213
IL2	0.906655	0.60929	1.349151	0.041028
TERT	0.948766	0.805797	1.117102	0.047995
FOS	0.964111	0.887687	1.047115	0.051878
MYC	1.076847	0.950394	1.220124	0.05602
ACD	0.88667	0.679283	1.157374	0.063411
UBE3A	1.054709	0.830352	1.339685	0.064208
BLM	1.098156	0.875418	1.377566	0.068383
MAPK1	0.957876	0.745733	1.23037	0.068448
RBBP7	0.927165	0.701126	1.226079	0.074303
SAP30	0.936982	0.739013	1.187983	0.090326
WT1	0.945065	0.818594	1.091075	0.097995
YWHAE	1.0101	0.778449	1.310686	0.099189
ATM	1.107862	0.89988	1.363913	0.109918
NBN	1.113041	0.8883	1.394642	0.129731
IFNAR2	1.053369	0.812793	1.365151	0.148204
IRF1	0.969776	0.838947	1.121008	0.151299
CDKN1B	1.043531	0.791294	1.376171	0.18565
SAP18	1.053654	0.767514	1.446472	0.19163
CCND1	1.030722	0.82032	1.295089	0.277829
SMAD3	0.972699	0.789202	1.198861	0.313892
XRCC6	1.020272	0.71548	1.454906	0.365676

KM (Kaplan Meier) Survival Analysis of TEASEs. (HR: Hazard Ratio, HR.95 L: HR95% confidence interval lower limit, HR.95 H: HR95% confidence interval upper limit, *p* < 0.05 is considered to be associated with survival prognosis)

321 DEGs, we corrected the p-values for multiple comparisons and presented them as q-values to provide a more precise assessment of the significance of the enrichment analysis outcomes. The findings indicated that DEGs were predominantly involved in biological processes such as cell differentiation, adhesion, and proliferation. Additionally, these DEGs were linked to cell components such as plasma and basement membrane. They were also found to be associated with the combination of substances in molecular functions (Fig. 4C). Furthermore, KEGG analysis revealed that DEGs were involved in multiple signaling pathways that had a critical role in tumor progression, such as PI3K-AKT, JAK-STAT, MAPK, and Ras signaling pathways (Fig. 4D).

Establishment and analysis of gene subclusters related to TEASEs

UniCox regression analysis was performed on the above DEGs to further select differential expression genes related to prognosis (DEGPs). Forty-one genes were successfully identified (Supplementary Table S1). Clustering analysis on these 41 DEGPs was subsequently performed. The most pronounced effect was observed when considering the cumulative function distribution at k=2. As a result, 781 prostate cancer patients were categorized into two distinct clusters (Cluster A and Cluster B) (Fig. 5A-B). The survival prognostic analysis plot suggested that Cluster B exhibited a better survival outcome than Cluster A (Fig. 5C). Similarly, the relationship between gene subclusters and the patients' attributes such as age, gleason score, and N/T stage using a heatmap (Fig. 5D). Additionally, the differential distribution of TEASEs in the two gene subclusters was plotted in a box plot, with the majority of the genes displaying higher expression in Cluster B compared to Cluster A (Fig. 5E).

Construction and analysis of the risk model for TEASEs

To better understand the significance of 41 DEGPs, prostate cancer patients in our study were randomly grouped into two cohorts, a test cohort, and a training cohort, in a 1:1 ratio. Following this, LASSO regression analysis was employed to construct a multi-cox regression risk model comprised of 9 genes, aiming to provide valuable prognostic insights (Fig. 6A-B). The formula for calculating the risk score is depicted as follows: Risk score = (−0.28357* FOSL2 expression) + (0.21214*KLF10 expression) + (−0.18548*SELL expression) + (−0.29501*SPARCL1 expression) + (0.48517*PLS3 expression) + (0.21560*ZWINT expression) + (−0.26450*ROBO1 expression) + (−0.24698*PDGFC expression) + (−0.21754*BANK1 expression). The relationships among the three TEASEs subgroups, two TEASEs gene clusters and two TEASEs risk groups were visually represented using a ggalluvial diagram (Fig. 6C).
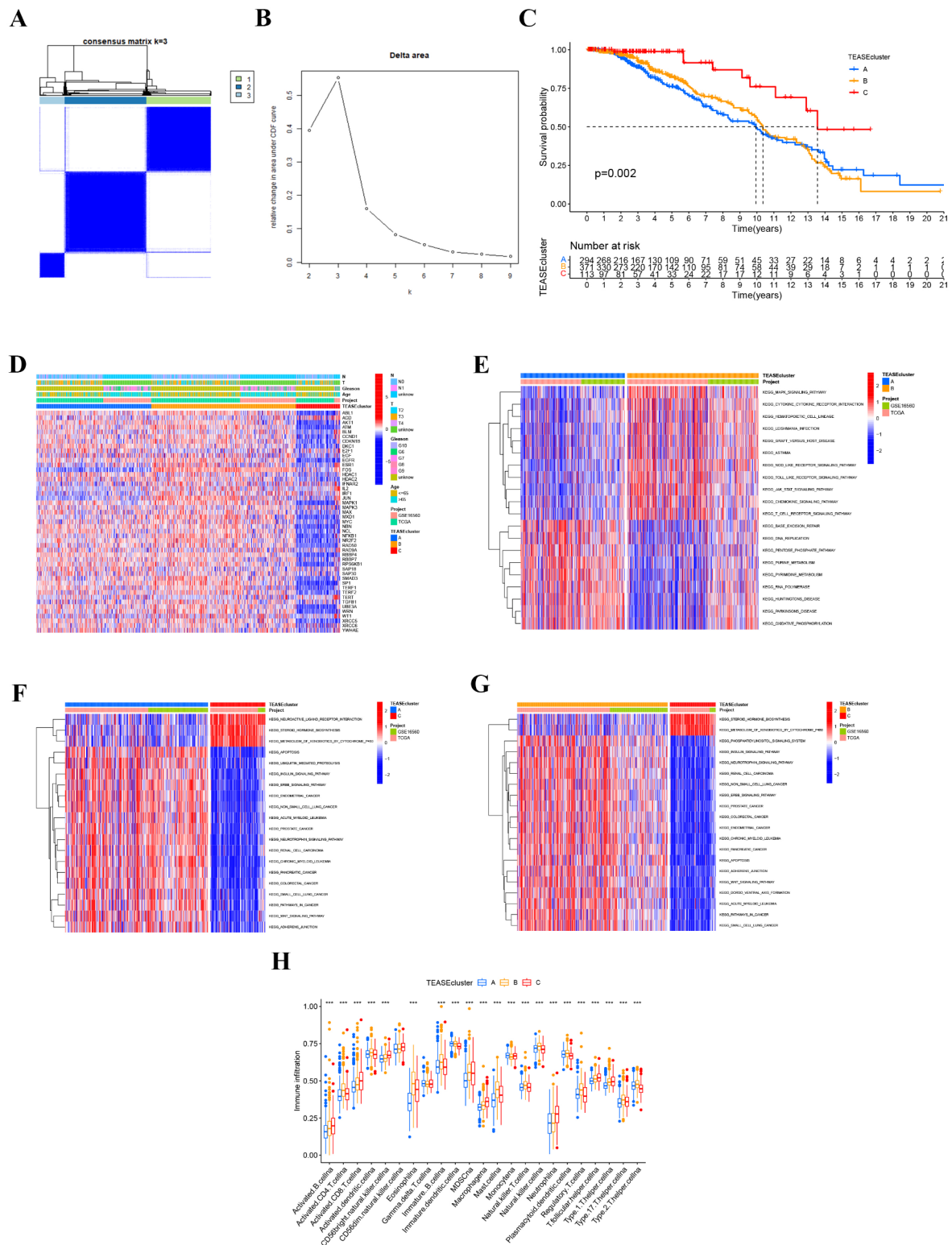
Fig. 3 TEASEs-associated molecular subtype characteristics. **(A)** Consensus Cluster Analysis for k = 3. **(B-C)** cumulative function distribution and survival analysis of 3 subtypes. **(D)** Expression profiles and clinicopathological feature correlations of different molecular subtypes. **(E-G)** KEGG pathway enrichment between A-B, A-C and B-C. **(H)** Differences in immune infiltration among molecular subtypes
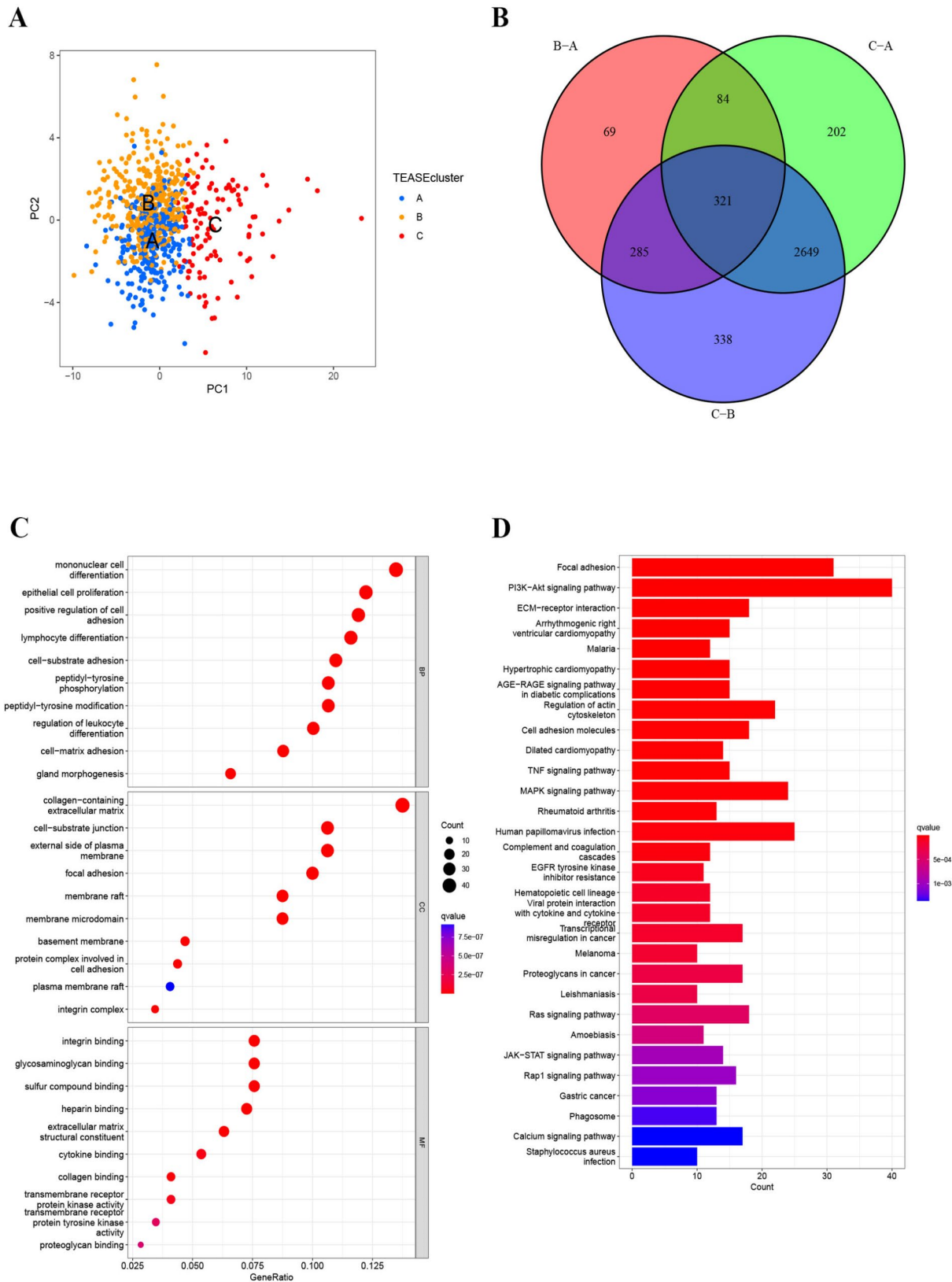
Fig. 4 Functional enrichment analysis of differentially expressed genes in different molecular subtypes. **(A)** principal component analysis. **(B)** Differential genes at the intersection of different molecular subtypes. **(C-D)** GO and KEGG analysis of differential genes among different molecular subtypes
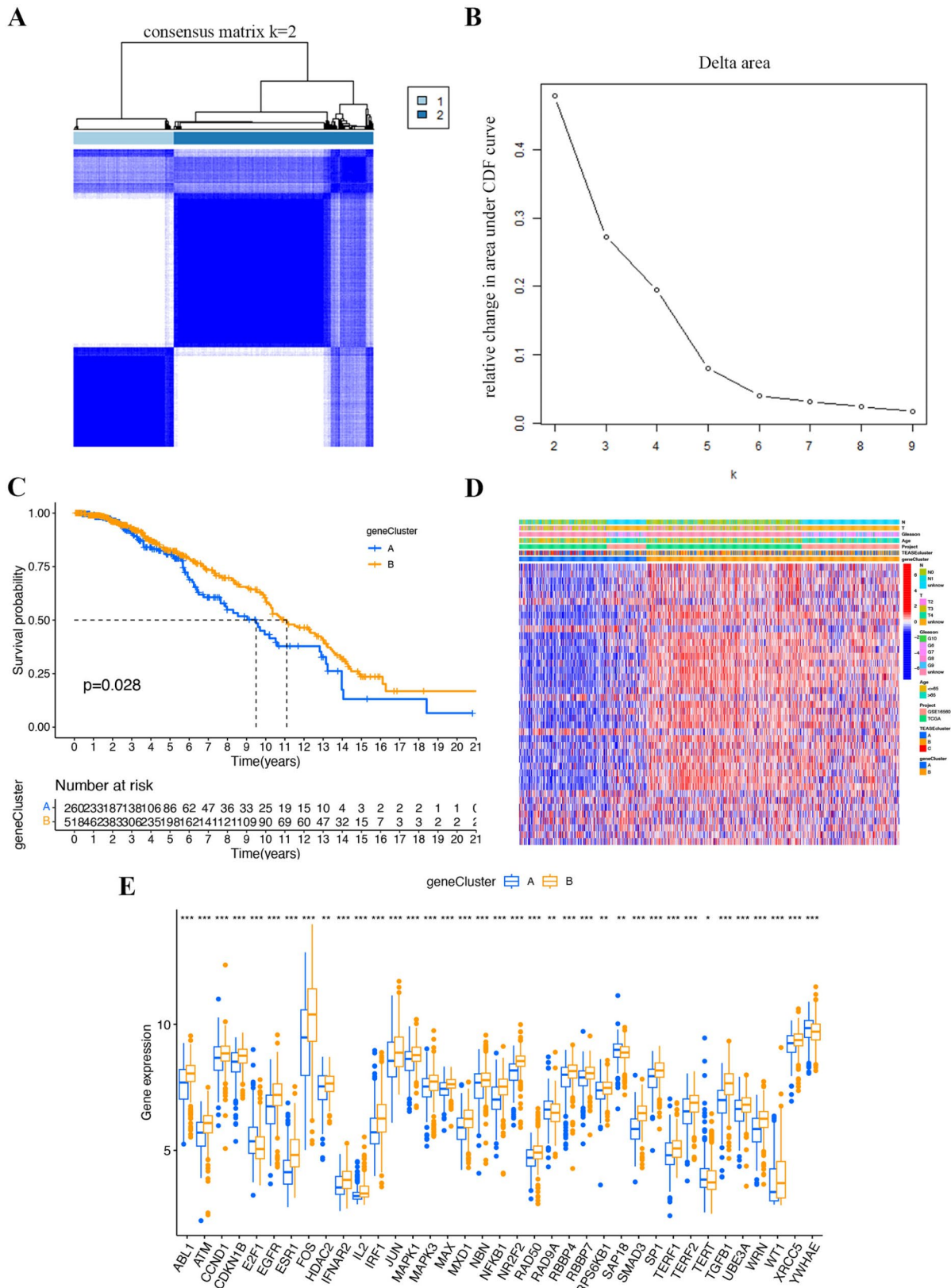
Fig. 5 Establishment and characterization of different gene subclusters of TEASEs. **(A)** Co-cluster analysis of differential genes related to prognosis. **(B)** The cumulative distribution function shows that k = 2 is the optimal number of subtypes. **(C)** Survival prognostic analysis of two gene subclusters. **(D)** Expression patterns of the 2 gene subclusters. **(E)** Differential expression of TEASEs between subcluster A and subcluster
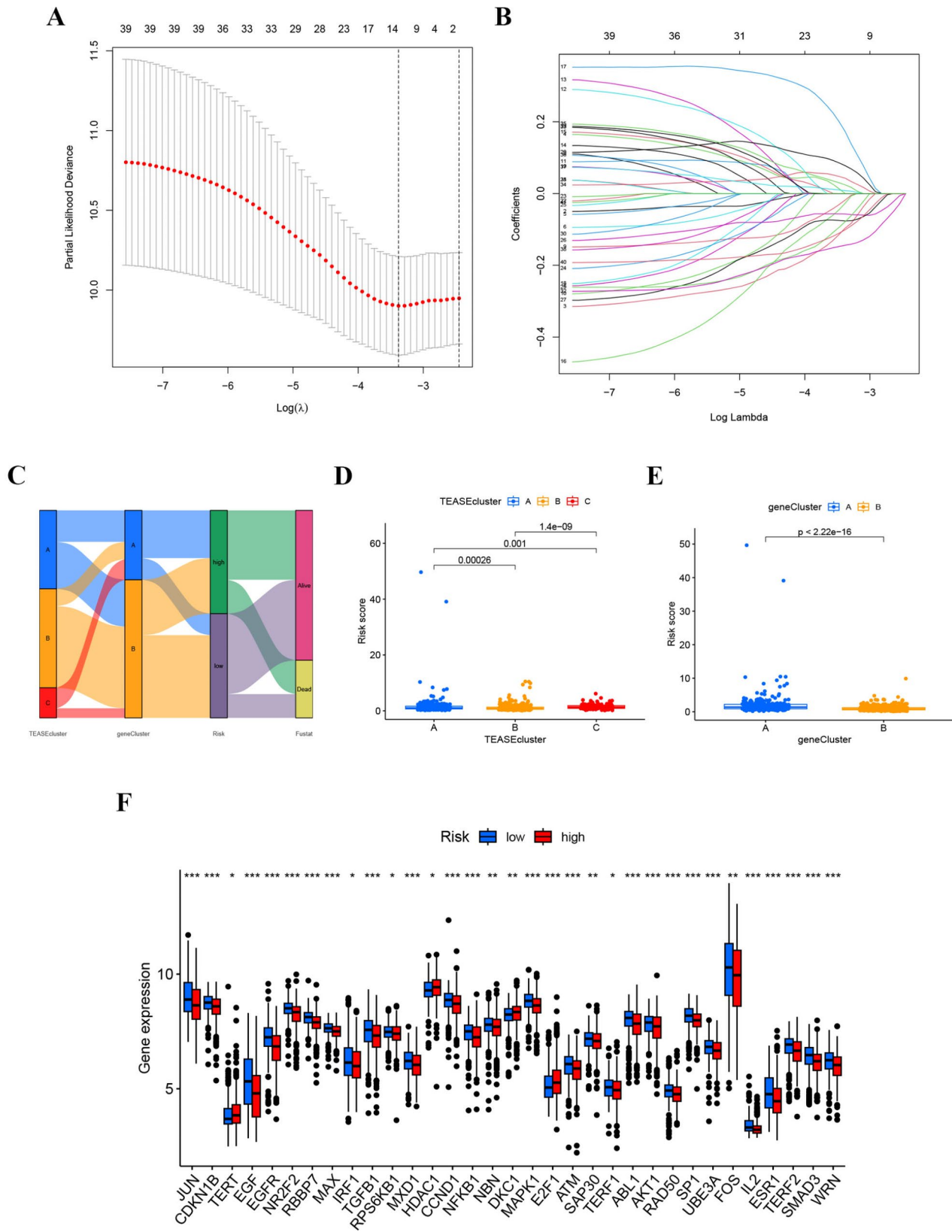
Fig. 6 Establishment of risk model. **(A-B)** LASSO regression for screening model genes. **(C)** Relationship between different molecular subtypes, gene subclusters, risk scores and survival prognosis. **(D-E)** The 3 Molecular subtypes and the 2 gene subclusters risk score differences. **(F)** Expression differences of TEASEs in different risk groups

Additionally, the risk score comparison of 3 TEASEs subgroups and 2 TEASEs gene subclusters was further shown in Fig. 6D-E. Furthermore, the variance analysis of TEASEs between high and low risk clusters was presented in a boxplot (Fig. 6F).

Survival prognostic analysis of the model

Survival prognosis exploration of general queue, training queue, and test queue was conducted, respectively. Differences in survival outcomes, survival status, survival ratio, risk score dispersion, and gene expression profile for each cohort were shown (Fig. 7A-R). It was revealed that the high-risk cluster was associated with more deaths and the worst survival prognosis of each cohort. We next evaluated the feature of the risk signature in terms of clinicopathologic factors (Age and Gleason score) for prostate cancer (Fig. 8A-C). The survival outcomes consistently favored the low-risk patients, surpassing those of the high-risk patients in all age groups (Age<=65 and Age>65). In addition, patients with a gleason score>7 exhibited a notably poorer survival outcome. To increase the generalizability of our risk model, we again validated the prognosis of biochemical recurrence in prostate cancer patients from GEO database (GSE54460) (Fig. 8D). The KM analysis also suggested that the high-risk patients had a higher likelihood of a biochemical recurrence. Next, we performed ROC curve plotting and GSEA analysis for different risk groups. The result was shown in the supplementary Figure S2. We found that WNT and TGFβ were enriched in the high-risk group, while JAK/STAT was enriched in the low-risk group. At the same time, the accuracy of survival prognosis for 3, 5 and 8 years was 0.642, 0.703 and 0.683.

Immunotherapy assessment of risk models

Previous studies have proved that cancer immunotherapy, particularly immune checkpoint inhibitors, has opened new horizons in tumor treatment. However, the efficacy of immunotherapy is affected by various factors, such as the infiltration of immune cells, particularly CD8 T cells, and immune checkpoint expression [8, 9]. The IME of different risk clusters was analyzed, revealing that the immune score and matrix score in the low-risk cluster were higher than those in the high-risk cluster (Fig. 8E). The endings of immune checkpoints suggested that the majority of the checkpoints were more enriched in the low-risk group, indicating that the low-risk patients may derive more substantial benefits from immunotherapy such as checkpoint inhibition (Fig. 8F). In the analysis of immune function, it was found that the low-risk group displayed a higher likelihood of being involved in the regulation of immune function than the high-risk group (Fig. 8G). The analysis of immune cell infiltration of model genes suggested that all 9 genes were associated with immune cells (Fig. 8H). Simultaneously, the majority of immune cells infiltration also presented an adverse association with our risk score (Fig. 8I). To further explore the value of the risk signature in immunotherapy, immunotherapy prognoses in the IMvigor210 cohort (Fig. 9A-E), the GSE78220 cohort (Fig. 9F-H), and the TCIA database (Fig. 9I-L) were verified. The patient's response to immunotherapy status was recorded as partial response (PR)/ complete response (CR), and progressive disease (PD)/stable disease (SD). In IMvigor210 cohort, the survival duration of all stage patients in the low-risk group was longer than those in the high-risk group (Fig. 9A), no matter for stage I-II (Fig. 9D) or stage III-IV patients (Fig. 9E). The curative effect of immunotherapy suggested that lower response rates were associated with higher risk scores (Fig. 9B), and the proportion of PD/SD patients in the high-risk group was also higher (Fig. 9C). In GSE78220 cohort, the prognosis in high-risk patient cohort was also poorer (Fig. 9F). Patients with a high-risk score were more likely to experience PD (Fig. 9G), while those achieving PR/CR were predominantly concentrated in the low-risk group (Fig. 9H). Upon acquiring immunotherapy data for prostate cancer from TCIA, it was evident that across various treatment modalities including single-agent anti-CTLA-4 or anti-PD-1 therapies, as well as combination therapy involving both strategies, patients within the low-risk group consistently demonstrated more substantial benefits (Fig. 9I-L).

Relevance analysis of risk characteristics and tumor mutagenicity and stemness

The TMB in patients of different risk status was compared. The high-risk group represented a higher mutation burden with a poorer prognosis, showing a positive correlation between risk score and TMB (Fig. 10A-C). Subsequently, the characteristics of somatic mutations in all patients of different risk status were explored. The findings revealed that the top six genes with the top mutation frequency in the high-risk cluster were SPOP, TP53, TTN, KMT2D, SPTA1, and MUC16, whereas SPOP, FOXA1, TTN, TP53, KMT2D and SYNE1 for the low-risk cluster (Fig. 10D-E). Cancer stem cells have previously been shown to have an important effect in the initiation, growth, and recurrence of prostate cancer [10]. In the stem analysis of risk groups, high-risk scores were generally associated with high tumor stemness (Fig. 10F).

Sensitivity analysis of chemotherapy drugs in different risk groups

According to the constructed model, the 'pRRophetic' package was utilized to assess the sensitivity of commonly used clinical or research drugs in prostate cancer. It was shown that bexarotene, bleomycin, bortezomib, dasatinib, erlotinib, etoposide, imatinib, lapatinib, nilotinib
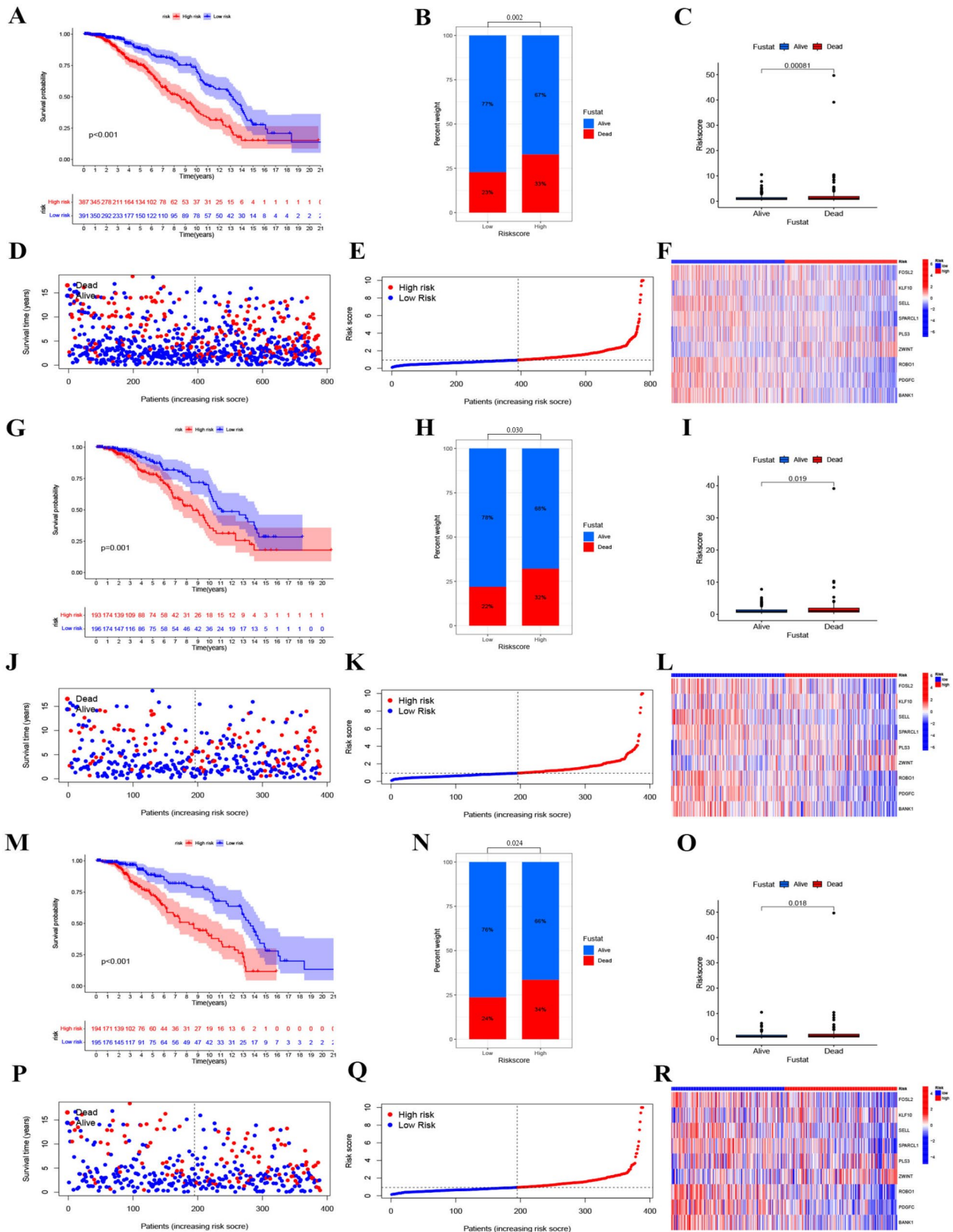
Fig. 7 Risk model survival prognosis. Survival analysis, survival proportions, survival status, risk score curves and gene expression heat maps for the **(A-F)** general cohort, **(G-L)** training cohort and **(M-R)** test cohort
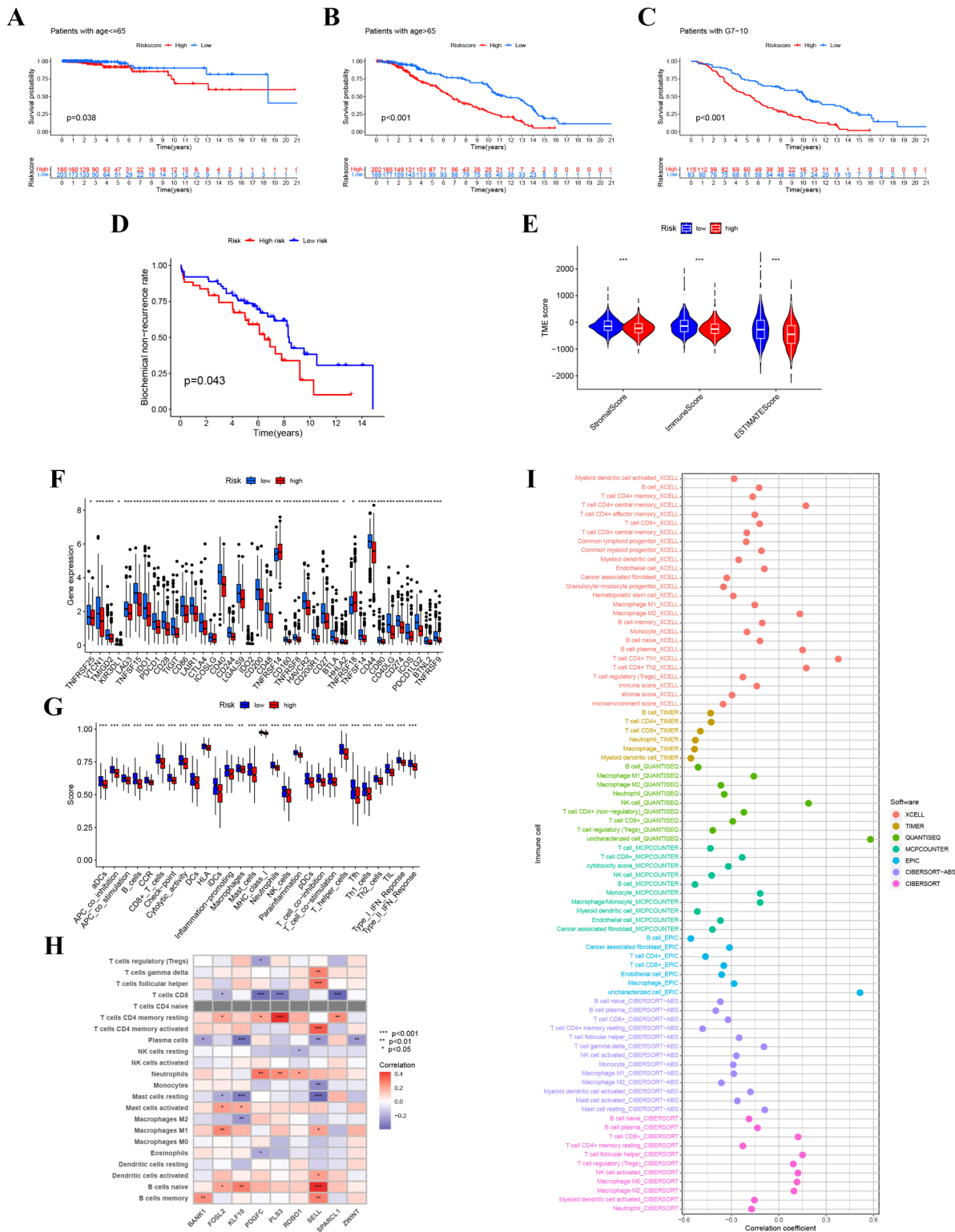
Fig. 8 Clinicopathological correlations and immune signatures in different risk groups. **(A)** age < 65, **(B)** age > 65, **(C)** Gleason7-10 and **(D)** biochemical recurrence comparison in high and low risk groups. **(E)** Differences in tumor microenvironment between high and low risk groups. **(F)** Expression of immune checkpoints in high and low risk groups. **(G)** Analysis of immune function in high and low risk groups. **(H)** Correlation between model genes and immune cell infiltration. **(I)** Correlation between risk score and immune cell infiltration
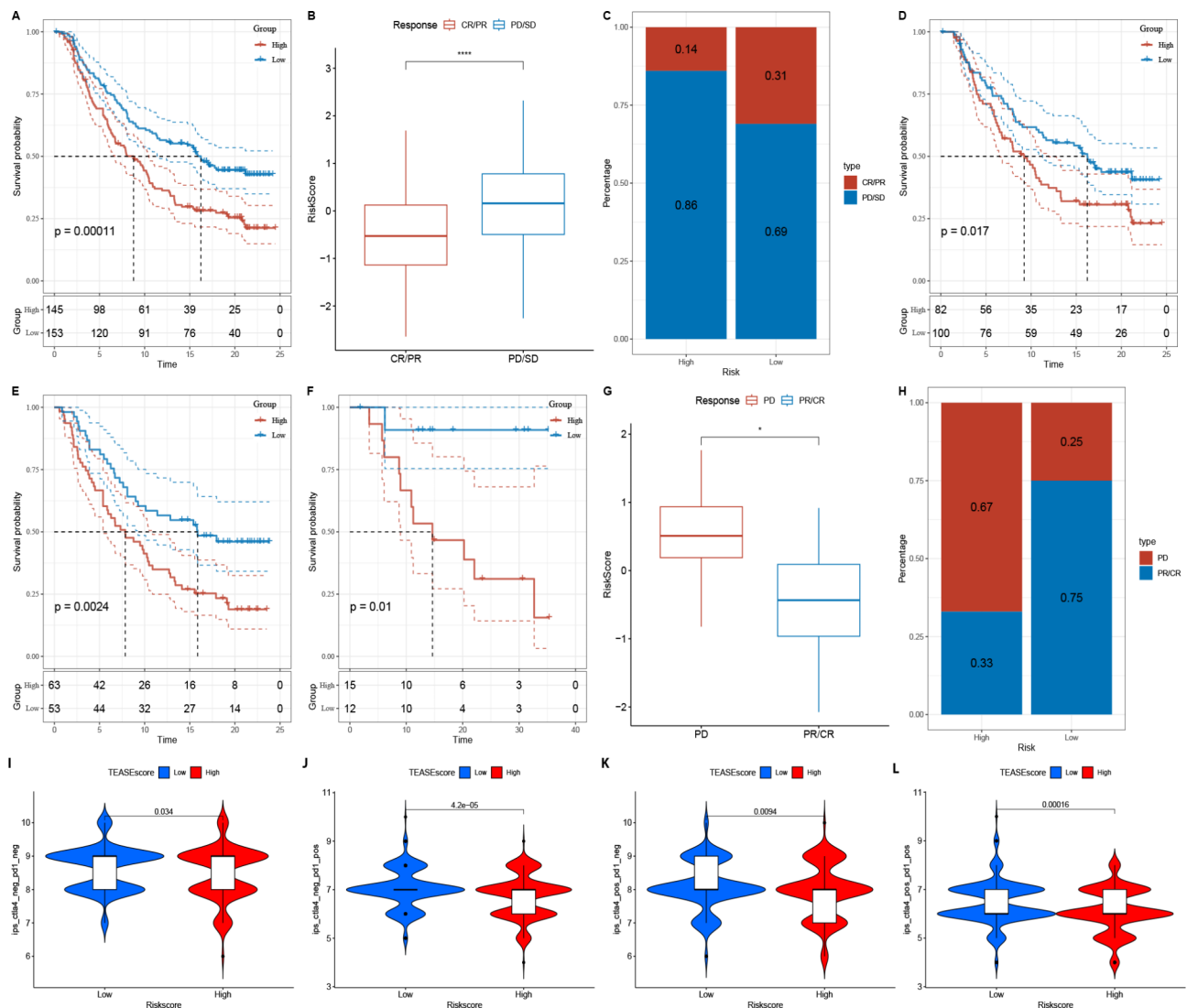
Fig. 9 Immunotherapy response in high- and low-risk groups. Survival prognosis of different risk groups in the IMvigor210 cohort in **(A)** all stages, **(D)** early stage, and **(E)** advanced stage. **(B-C)** IMvigor210 immunotherapy response status and distribution in different risk groups. **(F-H)** Survival prognosis, immunotherapy response status and distribution of different risk groups in the GSE78220 cohort. **(I-L)** Immune checkpoint inhibitor sensitivity analysis of four subtypes

and shikonin had a stronger sensitivity in the low-risk group, while camptothecin, cytarabine, docetaxel, metformin and vinblastine had smaller IC50 values in the high-risk group (Fig. 11). In summary, it was shown that the TEASEs model was closely related to drug sensitivity.

ZWINT as a novel marker contributing to prostate cancer diagnosis and prognosis

ZWINT was found enriched in the high-risk groups upon performing a differential expression analysis of the risk groups for model genes (Supplementary Figure S1), suggesting that ZWINT may have an essential role in prostate cancer progression. The immunohistochemistry results revealed that the quantity of ZWINT in prostate cancer tissues was significantly higher in comparison

to benign prostatic hyperplasia tissues (Fig. 12A). The analysis results in the UALCAN and GEPIA2 databases also proved that the quantity of ZWINT progressively increased with higher Gleason score in prostate cancer patients, which was associated with a poorer prognosis (Fig. 12B-D). Then, ZWINT single-cell analysis using the data from the TISCH2 database (GSE137829 (Fig. 13A and E) and GSE143791 (Fig. 13F and J)) was conducted. It was found that ZWINT was expressed in various types of cells, particularly malignant cells.

In summary, ZWINT had the prospect to become a new diagnostic and prognostic marker for prostate cancer. Such hypothesis was verified by in vitro experiments. The outcomes of western blot suggested that DU-145 and PC-3 exhibited the highest levels of ZWINT expression,

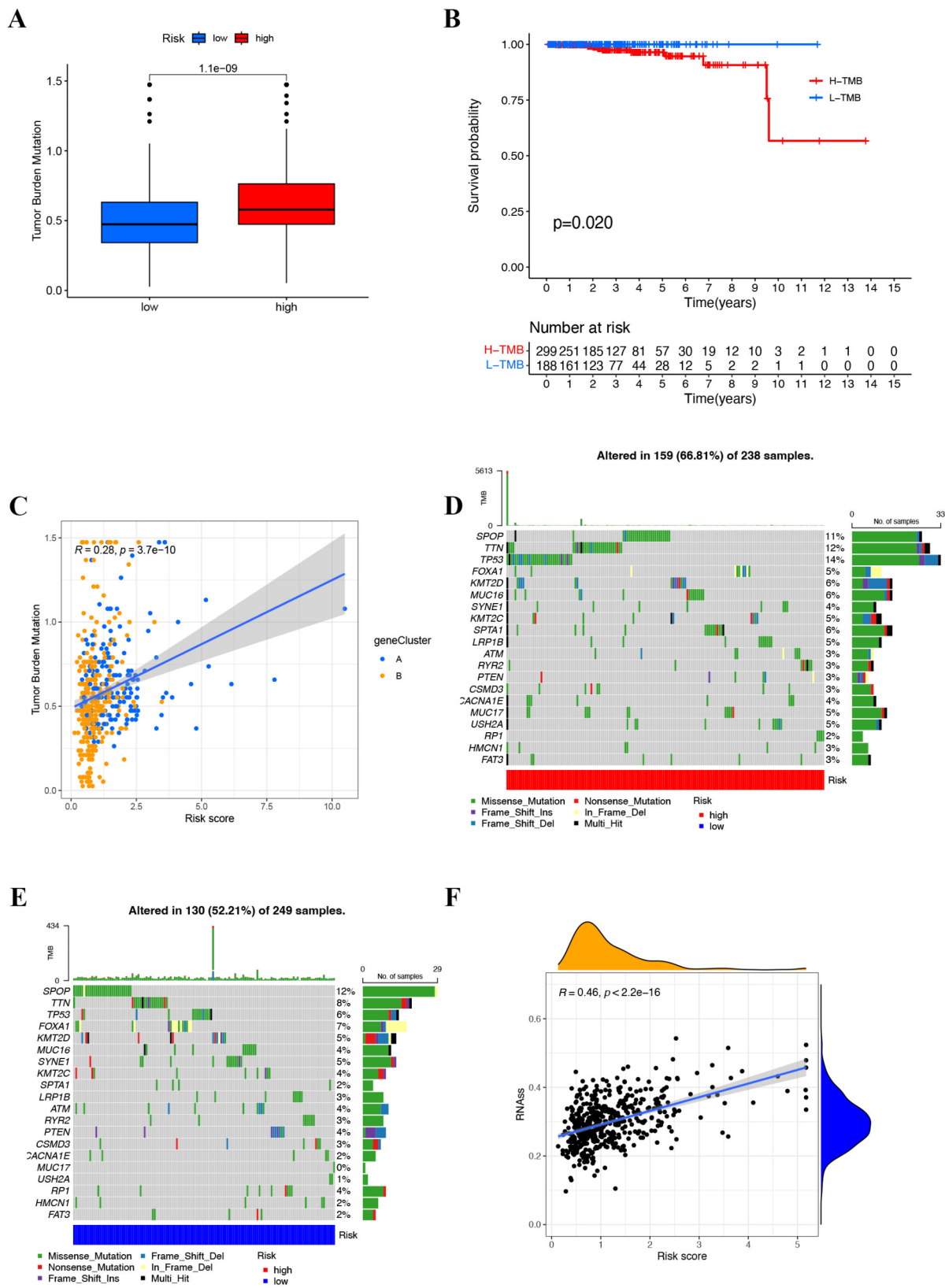**Fig. 10** Tumor mutation burden and stem cell correlation analysis. **(A-B)** Mutation burden and survival prognosis in different risk groups. **(C)** Correlation of risk scores with TMB. **(D-E)** Somatic mutation frequency in high-risk and low-risk groups. **(F)** Correlation analysis of risk score and cell stemness
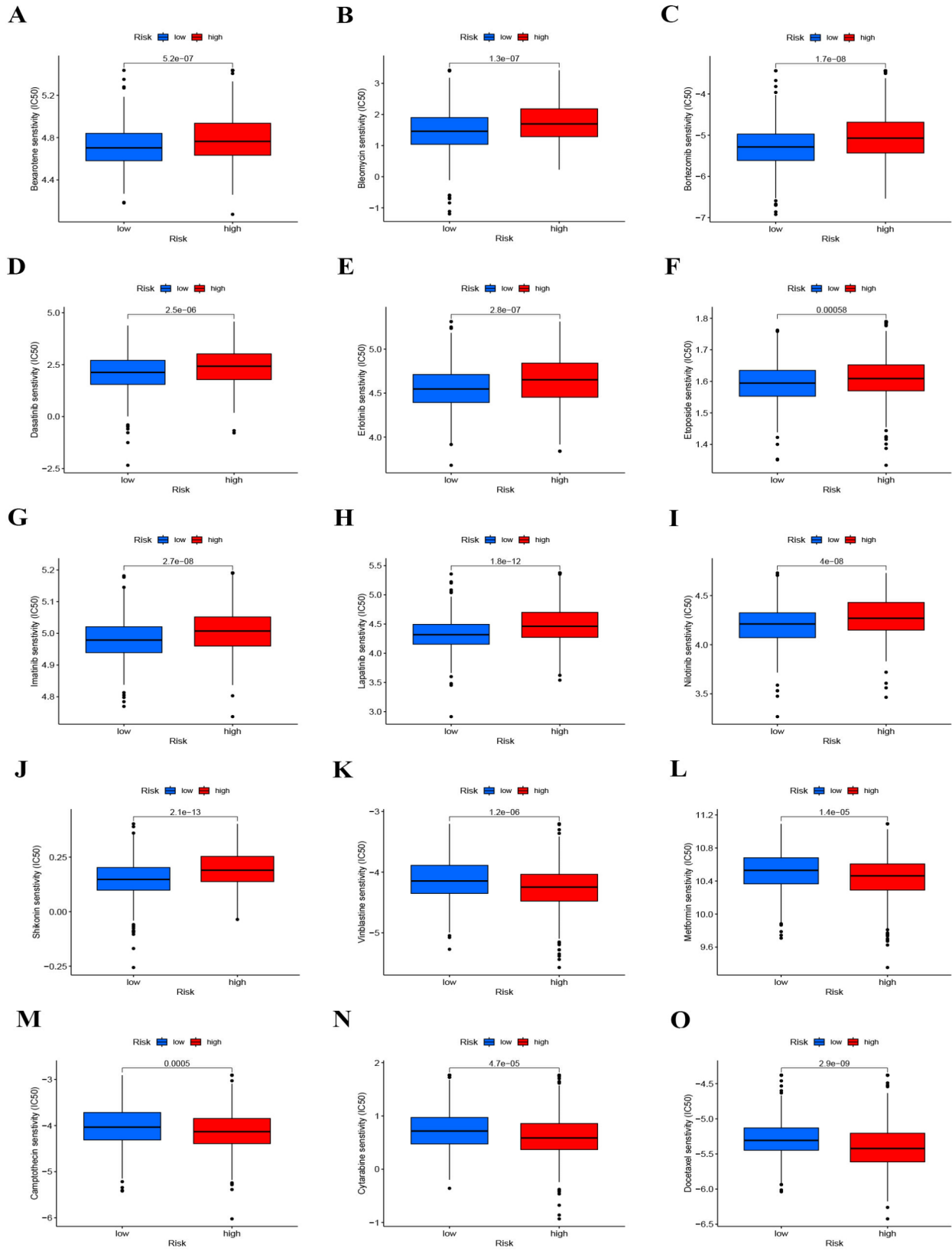
Fig. 11 Sensitivity analysis of chemotherapy drugs in different risk groups **(A-O)**.
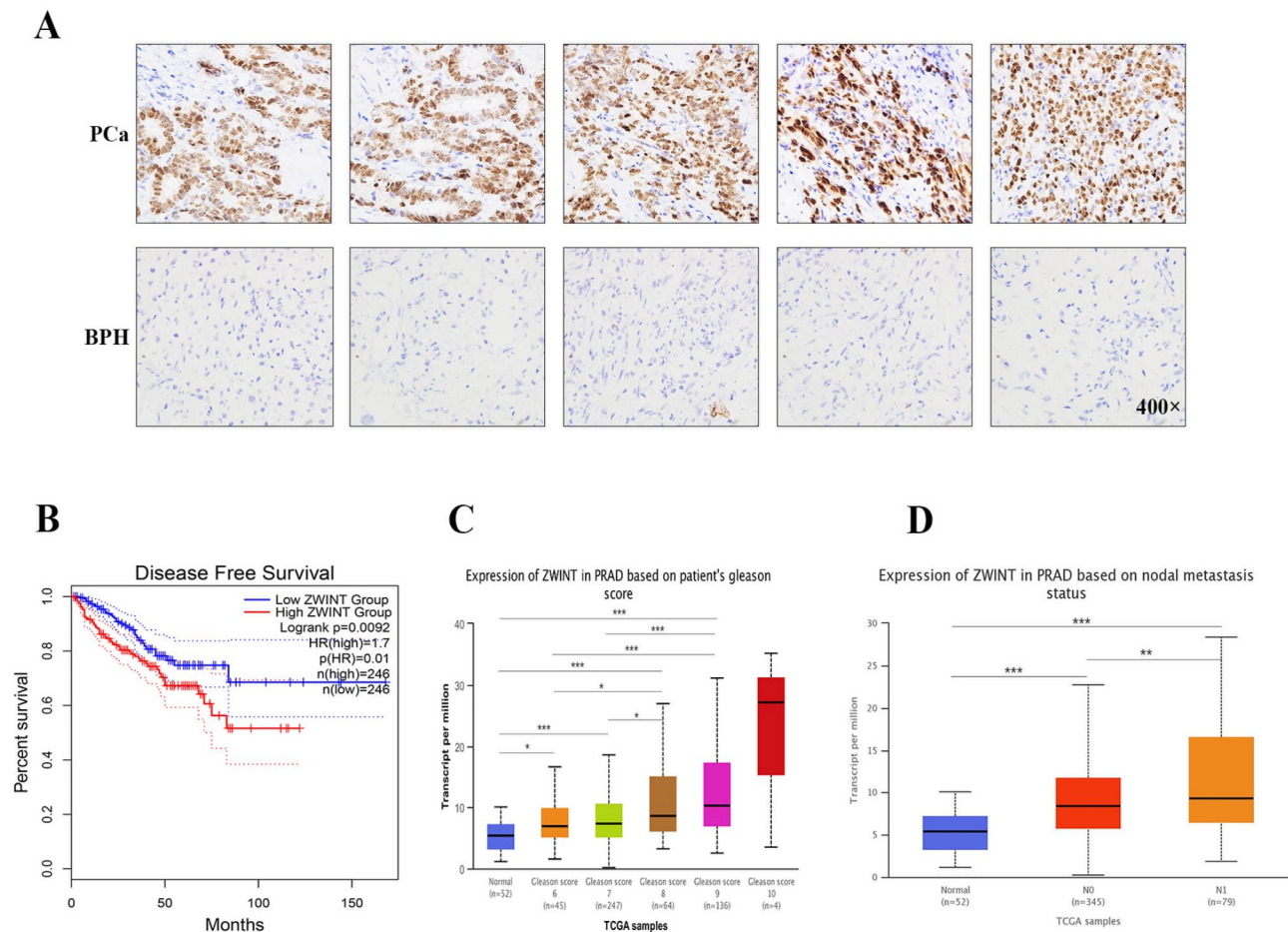
Fig. 12 Expression and survival significance of ZWINT in prostate cancer. **(A)** Immunohistochemical staining of ZWINT in tumor tissue and benign tissue. **(B-D)** Survival prognosis of ZWINT and its correlation with Gleason score and lymph node metastasis status. N0: No lymph node metastasis. N1: Lymph node metastasis

and the knockdown efficiency of si-ZWINT#1 and si-ZWINT#2 was also the highest (Fig. 14A-B). To investigate the proliferation impact of ZWINT, EDU and CCK-8 assays were performed. The findings suggested that the proliferation ability of cells treated with si-ZWINT#1 and si-ZWINT#2 was lower than that of in si-NC-treated group (Fig. 14C-D). We then further tested the invasion and migration effect of ZWINT in vitro. The results of transwell assay showed that the knockdown of ZWINT notably inhibited the invasion and migration ability of DU-145 and PC-3 in vitro (Fig. 14E-F). Overall, these outcomes revealed that ZWINT contributed to the malignant progression of prostate cancer.

ZWINT plays an essential role in prostate cancer growth and metastasis in vivo

To investigate the tumorigenic effect of ZWINT in vivo, ZWINT-KD and control PC3 cell lines were injected into mice subcutaneously to construct a xenograft model. The body weight of mice was measured every 2 days to monitor their growth (Fig. 15A). Fourteen days post injection,

it was shown that downregulation of ZWINT significantly reduced tumor weight and volume (Fig. 15B-E) and distant metastatic ability (Fig. 15F). These findings supported that ZWINT played a notable regulatory function in prostate cancer development in vivo.

Discussion

Currently, androgen deprivation therapy remains the primary treatment approach for prostate cancer. However, as the disease progresses, prostate cancer can evolve into castration-resistant prostate cancer (CRPC). CRPC is characterized by drug resistance, an increased risk of distant metastases, and a generally poorer prognosis, making it a challenging phase in the management of the disease [11–13]. Hence, it is indispensable to develop a reliable model to evaluate the prognosis and treatment outcome of prostate cancer patients.

Immunotherapy has revolutionarily transformed the treatment landscape for various types of cancer. However, prostate cancer today still shows limited sensitivity to immunotherapy due mainly to its classification as
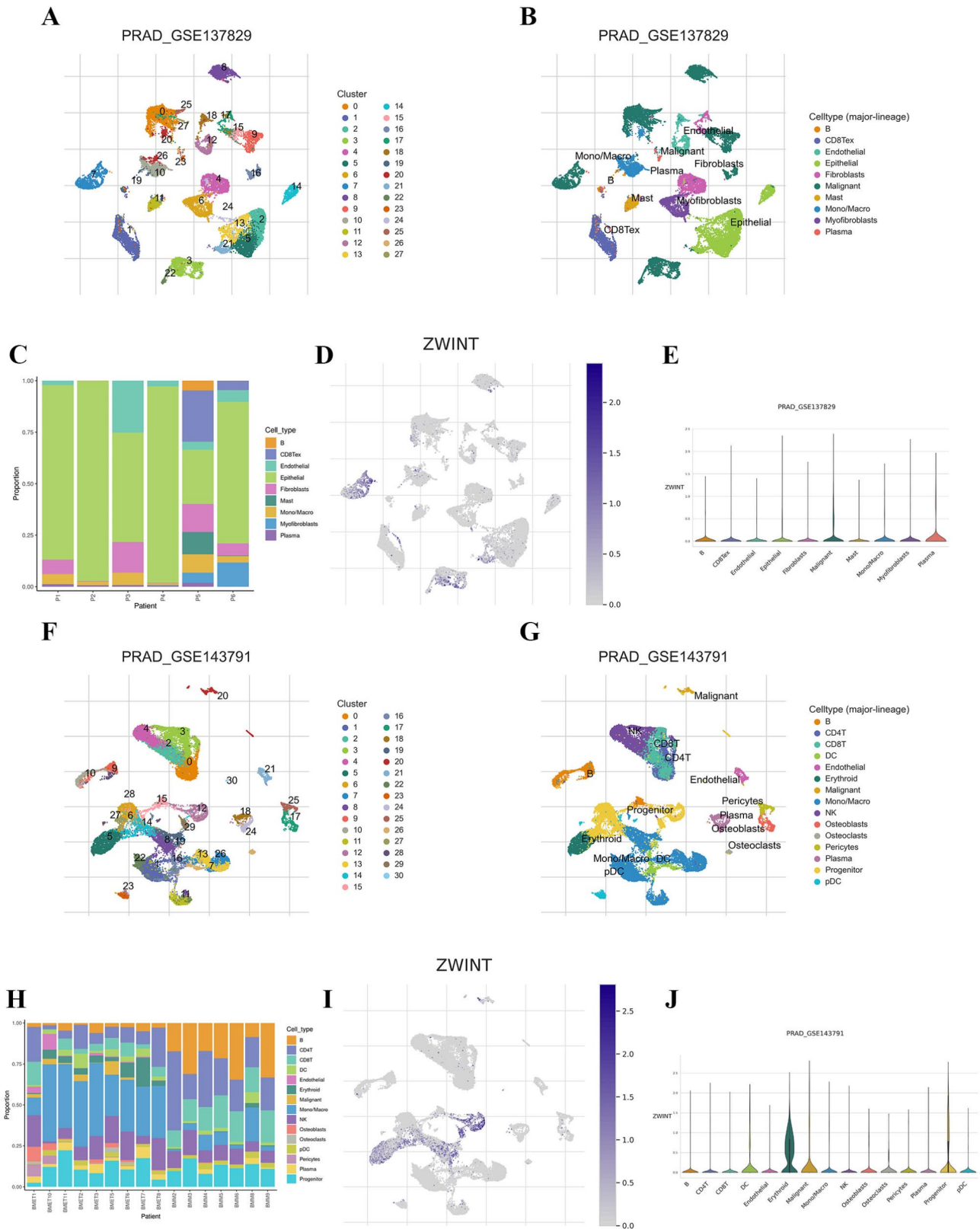
Fig. 13 ZWINT single cell data analysis. **(A-C)** GSE137829 associated subclusters, cell subtypes and cell subtype ratio. **(F-H)** GSE143791 associated subclusters, cell subtypes and cell subtype ratio. Distribution of ZWINT in **(D**, **I)** cell subclusters and **(E**, **J)** cell expression

Liu *et al. Cancer Cell International*   (2024) 24:294

Page 18 of 25
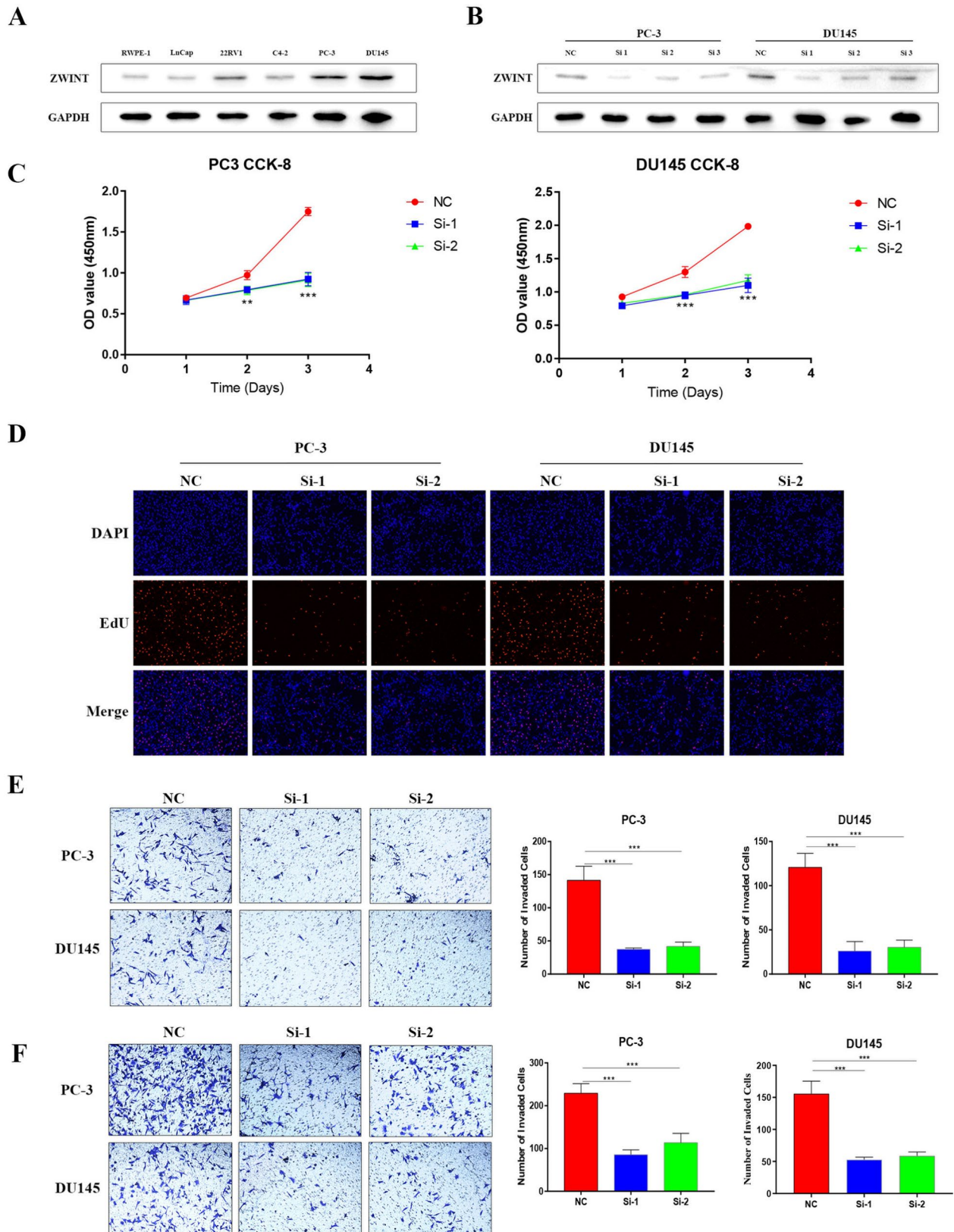
Fig. 14 ZWINT cell functional experiment. **(A)** Expression of ZWINT in prostate cancer cell lines. **(B)** ZWINT knockdown efficiency. **(C-D)** Cell proliferation experiment including CCK-8 and EDU. **(E-F)** Transwell assay to verify invasion and migration ability
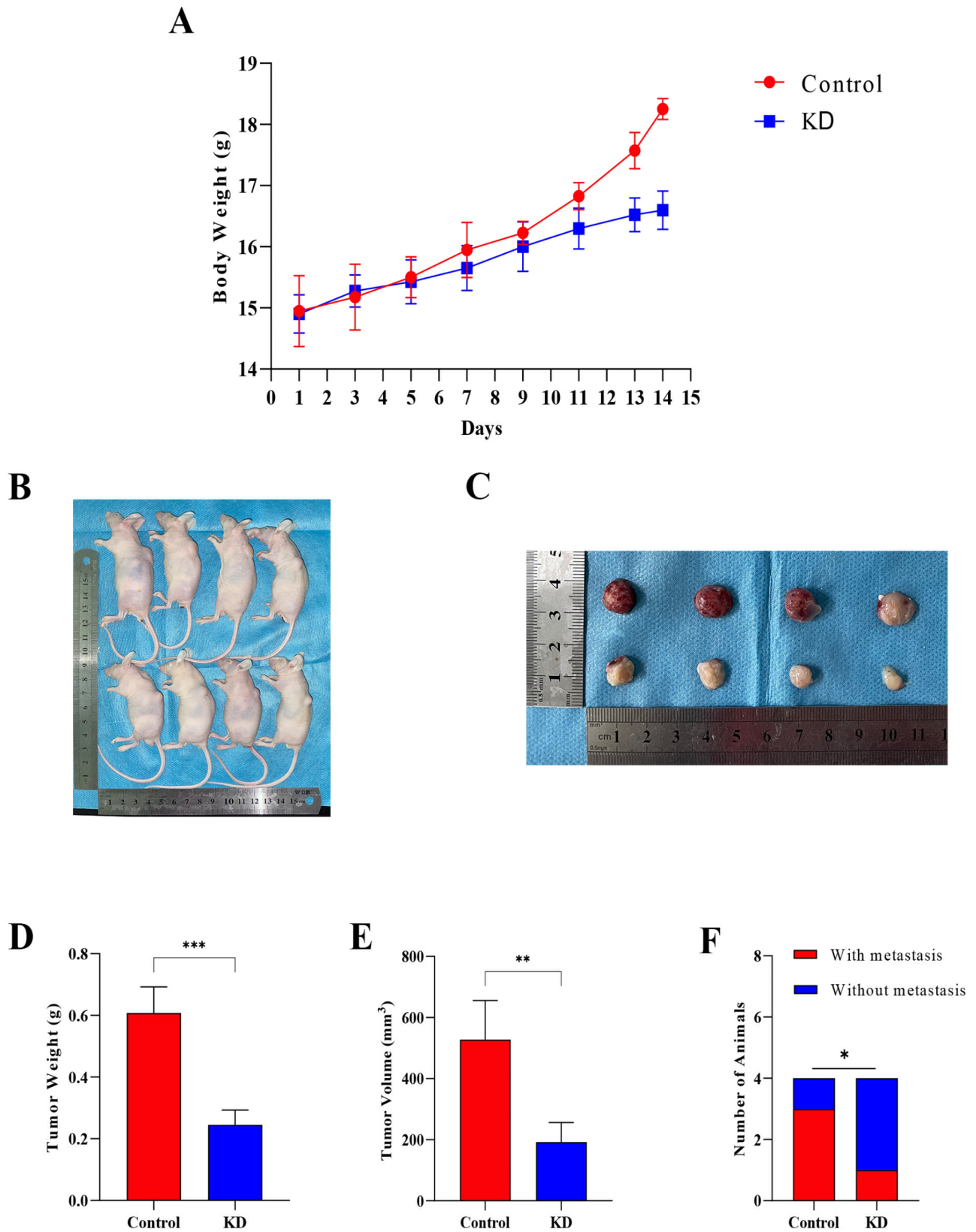
Fig. 15 Effect of ZWINT on tumorigenesis in mice. **(A)** Body weight change of nude mice. **(B-E)** Mass and volume of subcutaneous tumors in nude mice. **(F)** Metastatic status of cervical lymph nodes in two groups of nude mice

a "cold" tumor type. There is an urgent need to further understand the TME of prostate cancer and improve the immunotherapy outcome for it [14]. Although cellular aging and cancer development seem to be two distinct processes, they show close associations and interactions that are sophisticated with each other [15]. For example, telomerase serves as a shared mediator for aging and cancer [6]. Telomerase, with the main function to maintain the length of telomeres in cells, can interact with telomere and transform with telomere alternative lengthening mechanisms, thereby promoting cancer cell development [16]. Meanwhile, extremely shortened telomeres are positively correlated with increased instability of the genome and can promote early progression of cancer [6]. At present, the activation of telomerase can be used as a marker for most cancer types. The inhibition of telomerase activity is emerging as a new therapeutic strategy for cancer treatment, as it disrupts the maintenance telomere length in cancer cells, limiting tumor replication [17].

In the present study, specific molecular genetic alterations within TEASEs have been identified. A cluster analysis of TEASEs was performed to categorize distinct molecular subtypes. The biological process (BP), cell components (CC) and molecular functions (MF) of differential genes among different molecular subtypes were closely associated with cell and cell matrix adhesion. KEGG results showed that the above differential genes are related to PI3K-AKT and Ras signaling pathways. Previous studies have shown that abnormal adhesion of the vasculature and activation of the PI3K-AKT and Ras signaling pathways can affect the homing of T cells to tumors and thus affect the efficacy of immune checkpoint inhibitors (ICI) [18]. This further underscores the immunotherapeutic value of TEASEs. Following this, 41 key genes were obtained in differentially expressed genes from different molecular subtypes by uniCox prognostic analysis. We first established 2 gene subclusters through the above genes, and then obtained 9 model genes through LASSO regression and multiCox regression analysis.

The risk signature includes FOSL2, KLF10, SELL, SPARCL1, PLS3, ZWINT, ROBO1, PDGFC and BANK1. They were all associated with the malignant biological behavior of tumors. FOSL2 was reported to be responsible for VEGF-independent angiogenesis in breast cancer by activating Wnt5a in breast cancer-associated fibroblasts [19]. KLF10 serves as a tumor suppressor gene and can result in cancer cell apoptosis [20]. SELL can affect the immunotherapy prognosis of hepatocellular tumor via LINC00261/MiR105-5p/SELL pathways [21]. Overexpression of SPARCL1 in ovarian cancer can significantly inhibit the MEK/ERK pathways, thereby inhibiting the migration and proliferation of cells [22]. High PLS3

expression was reported to be associated with poorer prognosis of pancreatic cancer and contributes to cancer cell proliferation via PI3K/AKT pathways [23]. Under hypoxic conditions, ZWINT can activate the p53/p21 pathway to promote pancreatic cancer proliferation [24]. PRRG4 can downregulate ROBO1 in breast cancer, leading to the activation of protein tyrosine kinase Src and FAK and contributing to the migration of breast cancer cells [25]. PDGFC can induce liver fibrosis, lipoatrophy, and hepatocellular carcinoma [26]. BANK1 functions as a tumor suppressor for the development of B cell lymphoma [27].

Prognostic analysis results showed that patients in the high-risk group had worse survival prognosis and higher chances of biochemical recurrence. Subsequently, we compared the expression distribution of model genes in risk groups and found that ZWINT was abundantly enriched in the high-risk group. This suggested that ZWINT was a high-risk factor in the progression of prostate cancer. We explored the level expression of ZWINT in prostate cancer, and the results from immunohistochemistry suggested that ZWINT was enriched in cancer tissues to a higher extent than benign tissues. In single-cell data analysis, it was also observed that ZWINT expression was enriched in malignant tumor cells. In addition, the findings of GEPIA2 and UALCAN revealed that ZWINT had a worse prognosis and was closely related to the Gleason score. Meanwhile, in vitro and in vitro experiments showed that interference with the expression of ZWINT can lead to the inhibition of cancer cell proliferation, migration and invasion.

The current role of telomerase as a broad tumor-associated antigen facilitates telomerase-targeted immunotherapy [28]. In particular, the reverse transcriptase in telomerase which serves as a tumor target antigen, is expressed in more than 85% of the malignancies, although it is also found in normal cells such as testicular cells, hematopoietic stem cells and activated lymphocytes [29]. Therefore, telomerase may be a good immunotherapy target with a wide coverage. Subsequently, immune correlation analysis on the telomerase signature gene was performed. Significant differences in immune scores, stromal scores across different risk groups were found, indicating that the genetic signature can effectively assess the composition of prostate cancer TME. Immune cells in the TME play an important role in tumor development, affecting the outcome of immunotherapy [30]. In the following immune cell infiltration assay, the model genes were all found to be associated with immune cell infiltration. We found that M2 macrophages were enriched in the high-risk group, and M2 macrophages have been reported to predict poor prognosis in prostate cancer. This is also consistent with the prognosis of our high-risk group [31]. At the same time, the risk score was

inversely correlated with the infiltration of most immune cells, especially CD8 T cells. In the analysis of immune function and the expression of immune checkpoints, we also found that the expression of T cell inhibitory checkpoints LAG3 and HAVCR2 (TIM3) in the low-risk group was significantly higher than that in the high-risk group. Taken together, these findings suggested that the tumors within the low-risk group were more likely to transform into "hot" tumors upon receiving immunotherapy, conferring better immune responses.

To validate this hypothesis, we downloaded the prostate cancer TCIA IPS data. The data suggested that the low-risk patients may be more sensitive to CTLA-4 or PD-1 inhibitors. The low-risk group in the IMvigor210 and GSE78220 cohorts also displayed a stronger antitumor response. In addition to immunotherapy, chemotherapy also had an essential effect in the treatment of tumors. We assessed the IC50 of chemotherapeutic drugs in different risk groups and identified the specific chemotherapeutic agents to which prostate cancer in these groups exhibited sensitivity. TMB is currently considered a novel marker for assessing the response to immunotherapy. High TMB indicates a stronger immunogenicity, which can bolster anti-tumor immune responses [32]. We evaluated TMB and somatic mutation frequency in different risk groups. Interestingly, despite the low TMB levels exhibited by low-risk group, the low-risk group derived greater benefits from immunotherapy. This outcome was likely to result from different factors. Firstly, not all patients with high TMB can benefit from immunotherapy, since not all neoantigens generated are immunogenic and confer protection [33]. Secondly, it was reported elsewhere that prostate cancer patients with low TMB but high CD8 T cell infiltration density can also benefit from immunotherapy [34]. We also found that SPOP, TP53 and KMT2D had higher mutation frequencies in all risk groups. The mutations of the above 3 genes have been shown to play an essential role in the occurrence and development of prostate cancer [35–37], indicating their great potential as molecular targets for prostate cancer treatment. In molecular classification of prostate cancer, Meng et al. reported different immune subtypes and molecular systems PMOC in prostate cancer [38, 39]. Among immune subtype classifications, the immunosuppressive subtype is characterized by WNT and TGF-β activation and has a low immunotherapy response rate. Our high-risk group shared the above-mentioned characteristics similar to the immunosuppressive subtype, whereas the low-risk group represented another immune-activated subtype. In the PMOC classification, PMOC1 has JAK/STAT3 activation and poor survival prognosis and is considered an immune-activated status with high expression of PD1/PD-L1 and CTLA4, which is similar to our low-risk group. The

low-risk group may benefit more from immunotherapy. PMOC2 is characterized by oxidative phosphorylation and has the worst prognosis, accompanied by a high tumor mutation burden represented by SPOP and TP53 mutations, which is similar to our high-risk group. Meng et al. also reported on the prognosis of prostate cancer models [40–42]. The accuracy of our model for 5-year survival prognosis is better than the performance of above existing models in GSE70768, TCGA-PRAD, and GSE116918, and the accuracy of 3-year survival prognosis is better than the performance of GSE116918. In summary, we constructed new TEASEs signatures to better predict prostate cancer prognosis. Tailoring treatment strategies based on the risk groups to which prostate cancer patients are assigned can help maximize the therapeutic benefits for each individual.

Materials and methods
Data sources and disposal
TEASEs were retrieved from the GSEA database (https://www.gsea-msigdb.org/gsea/index.jsp) (Supplementary Table S2) [43]. Files encompassing 553 cases of genome transcription data, 500 cases of clinical data and 487 cases of gene mutation data associated with prostate cancer were downloaded from the TCGA database (https://www.cancer.gov/ccg/research/genome-sequencing/tcga) [44]. Transcriptome data was converted from FPKM to TPM. Copy number alteration datum was retrieved from the UCSC Xena [45]. Subsequently, 281 cases of prostate cancer transcriptome data and clinical data (GSE16560) in the GEO database (https://www.ncbi.nlm.nih.gov/geo/) were merged with TCGA datum and used as a training queue and a test queue [46]. GSE54460 was used as an external validation cohort, whereas GSE78220 [47], IMvigor210 cohort [48] and the TCIA database (https://tcia.at/home) [49] were used to predict the response of different risk groups to immunotherapy. The cohort information was shown in Supplementary Table S3.

Molecular genetic changes in TEASEs
The 'maftools' package was used to visualize TEASEs mutation data and 'RCiros' package was used to visualize copy number changes in TEASEs on chromosomes. Then, wilcox test was used to analyze the differential expression levels of TEASEs in tumor samples and normal samples (p < 0.05 was considered statistically significant). TEASEs prognostic network diagram was drawn using 'igraph' package.

Establishment of molecular subtypes and gene subclusters related to TEASEs based on co-clustering analysis
K-means co-clustering analysis was performed using the 'ConsensusClusterPlus' package and classified 781 prostate cancer patients into 3 distinct molecular subtypes.

The ssGSEA algorithm was used to score the infiltration abundance of immune cells among different molecular subtypes according to immune cell gene sets (Supplementary Table S4) and their corresponding gene expression in different subtypes. The kruskal.test method was used to perform a differential analysis on the mean values of the scores where $p < 0.05$ was considered statistically significant. Subsequently, uniCox prognostic analysis of DEGs from different molecular subtypes was performed and DEGPs were obtained. Two gene subclusters was established by co-clustering analysis of DEGPs. The relationship between 3 molecular subtypes and 2 gene clusters and the clinicopathological features including N/T stage, gleason score and age were displayed in the form of heatmap. The 'survival' and 'survminer' packages were utilized to perform prognostic analysis in molecular and gene subclusters.

Analysis of biological functions among different molecular subtypes

The 'limma' package and 'ggplot2' package were used to conduct principal component analysis on three molecular subtypes to assess the rationality of the classification. GSVA analysis was used to identify enriched pathways among different molecular subtypes. To explore the different IME among molecular subtypes, ssGSEA analysis was also employed to analyze immune cell infiltration status in different subtypes. DEGs in three molecular subtypes was then screened based on the following standards: the fold change and adjusted p value were set at 1.2 and 0.05, respectively. Finally, the 'org.Hs.eg.db' and the 'enrichplot' packages were applied to perform GO and KEGG on the above differential genes to understand their related biological functions and pathways.

Establishment of risk model and prognostic analysis

Prostate cancer patients from TCGA-PRAD and GSE16560 were randomly divided into two cohorts, the training and test groups, with an equal 1:1 ratio. LASSO regression analysis on DEGPs was then performed using the 'glment' package to reduce the risk of overfitting, and finally multiCox regression analysis was employed to screen for telomerase-related model genes. The risk score for each patient was calculated using the following equation:

$$Risk\ score = \sum_{a=1}^{n} coef(gene^a) * exp(gene^a)$$

coef ($gene^a$) represents the gene-related risk coefficient and exp ($gene^a$) stands for the gene expression rating. The survival prognosis was compared across different groups based on the median risk score, encompassing survival status, survival ratio, and distribution of risk scores. The validation cohort was used to conduct biochemical recurrence prognostic analysis of the risk signature. The relationship between TEASEs-related molecular subtypes and gene subclusters and risk score was displayed in the form of a Sankey diagram through the 'ggalluvial' package.

Characteristics of the IME and prediction of the immunotherapy response in the risk signature

The immune infiltration status of the signature genes was evaluated using the CIBERSORT algorithm. The immune checkpoint expression analysis and immune-related function analysis was then performed for different risk groups. The ESTIMATE method was employed to evaluate the TME score consisting of immune and stromal scores. ssGSEA algorithm was used to calculate immune-related function scores for different risk groups based on immune function-related gene sets (Supplementary Table S5) and their corresponding gene expression in high and low-risk groups. The score level indicated the correlation strength with immune function. The wilcox. test method was used to perform a differential analysis on the mean values of the scores and the different expression level of immune checkpoint genes in different risk groups ($p < 0.05$ was considered statistically). To better explore the utility of the risk model for predicting immunotherapy response using checkpoint inhibitor as the main treatment approach, the performance of our model using immunotherapy cohort and external databases were validated.

Evaluation of tumor mutation, stemness, and drug sensitivity

The connection between TMB, cancer cell stemness, and risk score and used 'maftools' package were analyzed to evaluate the frequency of somatic mutations among various risk groups. Meanwhile, 'pRRophetic' package was employed to detect the IC50 of chemotherapy agents among patients of different risk groups to evaluate their sensitivity to different chemotherapy drugs.

Cell culturing

Prostate cancer cell lines were obtained from the Chinese Academy of Medical Sciences. In brief, 10% fetal calf serum (HAKATA) with 1% streptomycin and penicillin (100units/ml, Solarbio) was added to the basal RPMI1640 medium (Biological Industries). The incubator was maintained in a humid environment with a temperature of 37 °C under 5% CO_2.

Expression and survival analysis of ZWINT

Pathological tissues of prostate cancer and benign prostatic hyperplasia were selected to make paraffin embedding and sectioning. The immunohistochemical antibody

was obtained from Abcam (ab252950), and the DAB staining reagent was obtained from Zhongshan Jinqiao (ZLI-9018). Western blot was employed to detect the expression and knockdown of ZWINT. RIPA lysate with PMSF (100:1) was used to lyse cells at 4℃ for 60 minutes, followed by centrifuging the cells at 11,000 rpm for 20 minutes to obtain the entire protein. Protein density was determined using BSA kit (Solarbio). 10% SDS/PAGE gel was used for protein electrophoresis and transferred to a NC membrane. Bands were incubated with ZWINT-related antibodies (Abcam, ab252950) and GAPDH-related antibodies (Proteintech) overnight at 4℃. ECL kit (Solarbio) was used to detect the binding status of the secondary antibody conjugated to HRP. The si-ZWINT sequence is as follow: si-ZWINT#1 (5'-GCACGTAGA GGCCATCAAA-3'), and si-ZWINT#2 (5'- GAACCA GTGGCAGCTACAA-3'). NC was used as the negative control. The relationship between ZWINT and clinico-pathological parameters of prostate cancer was obtained from the UALCAN database (https://ualcan.path.uab. edu/index.html) [50], and the survival prognosis of ZWINT was obtained from the GEPIA2 database (http:// gepia2.cancer-pku.cn/#index) [51].

The expression level of ZWINT promotes the malignant biological behavior of prostate cancer cell lines

The single-cell data of ZWINT in prostate cancer was retrieved from the TISCH2 database (http://tisch.comp-genomics.org/) [52]. CCK-8 and EDU experiments were utilized to observe the regulation of ZWINT on the proliferation of PC-3 and DU145. Three groups of cells at a number of 2000 cells per well were spread and measured under the absorbance at 450 nm for 3 consecutive days using CCK-8 reagent (APExBIO). In the EDU experiment, 3 groups of cells were incubated with the EDU kit (Abbkine) and observed under a fluorescence microscope. Transwell assay was employed to validate the effect of ZWINT on migration and invasion ability of the cell lines. Matrix gel was poured into the upper chamber to verify the invasion ability, while PC-3 and DU145 cell lines were pre-starved for 12 h and then added to the upper plate. The 1640 medium with 10% serum was then added to the lower dish. After 48 h of cell culture, the upper plate was fixed using paraformaldehyde for 25 min and stained with 0.1% crystal violet for 15 min. The upper chamber matrixgel was removed, and the above steps were repeated to verify the transfer ability. For the scratch healing assay, cells were plated on a six-well plate and scratched with a pipette tip, then rinsed with PBS. Photos were taken under a microscope at 24 h and 48 h respectively.

Tumor xenografts in nude mice

ZWINT knockdown lentiviral vector was purchased from GenePharma and ZWINT knockdown was abbre-viated as ZWINT-KD. ZWINT-KD and control PC3 cell lines were used for mouse xenografting, and 5×106 PC3 cells were subcutaneously injected into the dorsal side of 8 BALB/c nude mice (4–6 weeks old, 4 mice/group). The body weight of the mice was measured every 2 days, and the tumor was removed from the mice 14 days post injection to measure the mass and volume (0.5 × Length × Width) of the tumor. Subsequently, cervical lymph node DNA extraction and amplification of human Alu sequence PCR were performed to investigate the status of distant metastases [53].

Data statistics and evaluation

The assessment and statistics of bioinformatics data were completed by R platform (R 4.1.3), and the cell counting and graphing were accomplished by ImageJ and Graph-Pad Prism version 7.0. *, **, *** indicate p value < 0.05, p value < 0.01 and p value < 0.001, respectively.

Conclusion

The risk characteristics associated with TEASEs pre-liminarily elucidated the molecular genetic changes of prostate cancer patients and effectively predicted the survival prognosis of patients. ZWINT, a high-risk group-enriched gene, promoted the malignant biologi-cal behavior of prostate cancer and had the potential to become a new diagnostic and prognostic marker. Impor-tantly, the risk profile further revealed the immune microenvironment and drug sensitivity for chemotherapy within prostate cancer patients. This information serves as a crucial foundation for the precise design of subse-quent immunotherapy and chemotherapy.

Abbreviations
TEASEs	Telomerase-related genes
TME	Tumor microenvironment
TMB	Tumor mutational burden
ZWINT	ZW10 interactor
IME	Immune microenvironments
DEGs	Differentially expressed genes
DEGPs	Differential expression genes related to prognosis
CRPC	Castration-resistant prostate cancer
ICI	Immune checkpoint inhibitors

Supplementary Material 1: Supplementary Figure S1: Differential expres-sion of telomerase related signature genes in different risk score groups.

Supplementary Material 2: Supplementary Table S1: Telomerase-associated prognostic differential gene (DEGPs). Supplementary Table S2: Telomerase-associated genes (TEASEs). Supplementary Table S3: Clinical characteristics of enrolled patients in each dataset. Supplementary Table S4: Immune cell

gene sets Supplementary Table S5: Immune function-related gene sets

Supplementary Material 3: Supplementary Figure S2: ROC curve plotting and GSEA analysis for different risk groups.

Author contributions
LD and QZ researched and all the analyses and drafted original manuscript. YB, XH and LY performed the experiment and data analysis. ZL and YK critically reviewed the manuscript. XY and ZH provided administrative, technical, and material support. All authors reviewed the manuscript.

Data availability
No datasets were generated or analysed during the current study.

Declarations

Ethics approval and consent to participate
The Medical Ethics Committee of the Second Hospital of Tianjin Medical University approved the experiments involving human tumor tissues (KY2023K144), and all patients signed the informed consent. The animal protocols were approved by the Institutional Animal Care and Use Committee of Yi Shengyuan Gene Technology (Tianjin) Co., Ltd. (protocol number YSY-DWLL-2023225), and all the animal experiments complied with the guidelines of the Tianjin Medical Experimental Animal Care.

Consent for publication
Informed consent for publication of identifiable images in open access journal was obtained from all study participants.

Competing interests
The authors declare no competing interests.

Author details
[1]Institute of Urology, The Second Hospital of Tianjin Medical University, Tianjin, China
[2]Department of Oncology, The Second Hospital of Tianjin Medical University, Tianjin, China

References
1. Hassanipour S, Delam H, Arab-Zozani M, Abdzadeh E, Hosseini SA, Nikbakht HA, Malakoutikhah M, Ashoobi MT, Fathalipour M, Salehiniya H, Riahi S. Survival rate of prostate Cancer in Asian countries: a systematic review and Meta-analysis. Ann Glob Health. 2020;86:2.
2. Kunath F, Grobe HR, Rücker G, Motschall E, Antes G, Dahm P, Wullich B, Meerpohl JJ. Non-steroidal antiandrogen monotherapy compared with luteinising hormone-releasing hormone agonists or surgical castration monotherapy for advanced prostate cancer. Cochrane Database Syst Rev. 2014;:CD009266.
3. Litwin MS, Tan HJ. The diagnosis and treatment of prostate Cancer: a review. JAMA. 2017;317:2532–42.
4. Sekhoacha M, Riet K, Motloung P, Gumenku L, Adegoke A, Mashele S. Prostate Cancer Review: Genetics, diagnosis, Treatment options, and alternative approaches. Molecules. 2022;27:5730.
5. Sandhu S, Moore CM, Chiong E, Beltran H, Bristow RG, Williams SG. Prostate cancer. Lancet. 2021;398:1075–90.
6. Bernardes de Jesus B, Blasco MA. Telomerase at the intersection of cancer and aging. Trends Genet. 2013;29:513–20.
7. Shay JW, Zou Y, Hiyama E, Wright WE. Telomerase and cancer. Hum Mol Genet. 2001;10:677–85.
8. Petitprez F, Meylan M, de Reyniès A, Sautès-Fridman C, Fridman WH. The Tumor Microenvironment in the response to Immune Checkpoint Blockade therapies. Front Immunol. 2020;11:784.
9. Liu D, Xu S, Chang T, Ma S, Wang K, Sun G, Chen S, Xu Y, Zhang H. Predicting prognosis and distinguishing cold and hot tumors in bladder Urothelial Carcinoma based on Necroptosis-Associated lncRNAs. Front Immunol. 2022;13:916800.
10. Escudero-Lourdes C, Alvarado-Morales I, Tokar EJ. Stem cells as target for prostate cancer therapy: opportunities and challenges. Stem Cell Rev Rep. 2022;18:2833–51.
11. Chow H, Ghosh PM, deVere White R, Evans CP, Dall'Era MA, Yap SA, Li Y, Beckett LA, Lara PN Jr, Pan CX. A phase 2 clinical trial of everolimus plus bicalutamide for castration-resistant prostate cancer. Cancer. 2016;122:1897–904.
12. Sidaway P. Prostate cancer: Enzalutamide is superior to bicalutamide for mCRPC. Nat Rev Urol. 2016;13:124.
13. Moreira DM, Howard LE, Sourbeer KN, Amarasekara HS, Chow LC, Cockrell DC, Pratson CL, Hanyok BT, Aronson WJ, Kane CJ, Terris MK, Amling CL, Cooperberg MR, et al. Predicting Time from Metastasis to overall survival in castration-resistant prostate Cancer: results from SEARCH. Clin Genitourin Cancer. 2017;15:60–e662.
14. Nair SS, Weil R, Dovey Z, Davis A, Tewari AK. The Tumor Microenvironment and Immunotherapy in prostate and bladder Cancer. Urol Clin North Am. 2020;47:e17–54.
15. Campisi J. Aging, cellular senescence, and cancer. Annu Rev Physiol. 2013;75:685–705.
16. De Vitis M, Berardinelli F, Sgura A. Telomere length maintenance in Cancer: at the crossroad between Telomerase and Alternative Lengthening of telomeres (ALT). Int J Mol Sci. 2018;19:606.
17. Zvereva MI, Shcherbakova DM, Dontsova OA. Telomerase: structure, functions, and activity regulation. Biochem (Mosc). 2010;75:1563–83.
18. Liu YT, Sun ZJ. Turning cold tumors into hot tumors by improving T-cell infiltration. Theranostics. 2021;11:5365–86.
19. Wan X, Guan S, Hou Y, Qin Y, Zeng H, Yang L, Qiao Y, Liu S, Li Q, Jin T, Qiu Y, Liu M. FOSL2 promotes VEGF-independent angiogenesis by transcriptionally activating Wnt5a in breast cancer-associated fibroblasts. Theranostics. 2021;11:4975–91.
20. Memon A, Lee WK. KLF10 as a tumor suppressor Gene and its TGF-β signaling. Cancers (Basel). 2018;10:161.
21. Song H, Huang XF, Hu SY, Lu LL, Yang XY. The LINC00261/MiR105-5p/SELL axis is involved in dysfunction of B cell and is associated with overall survival in hepatocellular carcinoma. PeerJ. 2022;10:e12588.
22. Ma Y, Xu Y, Li L. SPARCL1 suppresses the proliferation and migration of human ovarian cancer cells via the MEK/ERK signaling. Exp Ther Med. 2018;16:3195–201.
23. Xin Z, Li D, Mao F, Du Y, Wang X, Xu P, Li Z, Qian J, Yao J. PLS3 predicts poor prognosis in pancreatic cancer and promotes cancer cell proliferation via PI3K/AKT signaling. J Cell Physiol. 2020;235:8416–23.
24. Chen P, He Z, Wang J, Xu J, Jiang X, Chen Y, Liu X, Jiang J. Hypoxia-Induced ZWINT mediates pancreatic Cancer proliferation by interacting with p53/p21. Front Cell Dev Biol. 2021;9:682131.
25. Zhang L, Qin Y, Wu G, Wang J, Cao J, Wang Y, Wu D, Yang K, Zhao Z, He L, Lyu J, Li H, Gu H. PRRG4 promotes breast cancer metastasis through the recruitment of NEDD4 and downregulation of Robo1. Oncogene. 2020;39:7196–208.
26. Campbell JS, Hughes SD, Gilbertson DG, Palmer TE, Holdren MS, Haran AC, Odell MM, Bauer RL, Ren HP, Haugen HS, Yeh MM, Fausto N. Platelet-derived growth factor C induces liver fibrosis, steatosis, and hepatocellular carcinoma. Proc Natl Acad Sci U S A. 2005;102:3389–94.
27. Yan J, Nie K, Mathew S, Tam Y, Cheng S, Knowles DM, Orazi A, Tam W. Inactivation of BANK1 in a novel IGH-associated translocation t(4;14)(q24;q32) suggests a tumor suppressor role in B-cell lymphoma. Blood Cancer J. 2014;4:e215.
28. Vonderheide RH. Telomerase as a universal tumor-associated antigen for cancer immunotherapy. Oncogene. 2002;21:674–9.
29. Mizukoshi E, Kaneko S. Telomerase-targeted Cancer Immunotherapy. Int J Mol Sci. 2019;20:1823.
30. Lei X, Lei Y, Li JK, Du WX, Li RG, Yang J, Li J, Li F, Tan HB. Immune cells within the tumor microenvironment: Biological functions and roles in cancer immunotherapy. Cancer Lett. 2020;470:126–33.

31. Meng J, Liu Y, Guan S, Fan S, Zhou J, Zhang M, Liang C. The establishment of immune infiltration based novel recurrence predicting nomogram in prostate cancer. Cancer Med. 2019;8(11):5202–13.
32. Wang L, Pan S, Zhu B, Yu Z, Wang W. Comprehensive analysis of tumour mutational burden and its clinical significance in prostate cancer. BMC Urol. 2021;21:29.
33. Chabanon RM, Pedrero M, Lefebvre C, Marabelle A, Soria JC, Postel-Vinay S. Mutational Landscape and Sensitivity to Immune Checkpoint blockers. Clin Cancer Res. 2016;22:4309–21.
34. Subudhi SK, Vence L, Zhao H, Blando J, Yadav SS, Xiong Q, Reuben A, Aparicio A, Corn PG, Chapin BF, Pisters LL, Troncoso P, Tidwell RS, et al. Neoantigen responses, immune correlates, and favorable outcomes after ipilimumab treatment of patients with prostate cancer. Sci Transl Med. 2020;12:eaaz3577.
35. Shi Q, Jin X, Zhang P, Li Q, Lv Z, Ding Y, He H, Wang Y, He Y, Zhao X, Zhao SM, Li Y, Gao K, et al. SPOP mutations promote p62/SQSTM1-dependent autophagy and Nrf2 activation in prostate cancer. Cell Death Differ. 2022;29:1228–39.
36. Zhang Y, Song XL, Yu B, Foong LC, Shu Y, Mai CW, Hu J, Dong B, Xue W, Chua CW. TP53 loss-of-function causes vulnerability to autophagy inhibition in aggressive prostate cancer. Int J Urol. 2022;29:1085–94.
37. Lv S, Ji L, Chen B, Liu S, Lei C, Liu X, Qi X, Wang Y, Lai-Han Leung E, Wang H, Zhang L, Yu X, Liu Z, Wei Q, Lu L. Histone methyltransferase KMT2D sustains prostate carcinogenesis and metastasis via epigenetically activating LIFR and KLF4. Oncogene. 2018;37:1354–68.
38. Meng J, Zhou Y, Lu X, Bian Z, Chen Y, Zhou J, Zhang L, Hao Z, Zhang M, Liang C. Immune response drives outcomes in prostate cancer: implications for immunotherapy. Mol Oncol. 2021;15(5):1358–75.
39. Meng J, Lu X, Jin C, Zhou Y, Ge Q, Zhou J, Hao Z, Yan F, Zhang M, Liang C. Integrated multi-omics data reveals the molecular subtypes and guides the androgen receptor signalling inhibitor treatment of prostate cancer. Clin Transl Med. 2021;11(12):e655.
40. Meng J, Guan Y, Wang B, Chen L, Chen J, Zhang M, Liang C. Risk subtyping and prognostic assessment of prostate cancer based on consensus genes. Commun Biol. 2022;5(1):233.
41. Meng J, Lu X, Zhou Y, Zhang M, Gao L, Gao S, Yan F, Liang C. Characterization of the prognostic values and response to immunotherapy/chemotherapy of Krüppel-like factors in prostate cancer. J Cell Mol Med. 2020;24(10):5797–810.
42. Gao L, Meng J, Zhang Y, Gu J, Han Z, Wang X, Gao S. Development and validation of a six-RNA binding proteins prognostic signature and candidate drugs for prostate cancer. Genomics. 2020;112(6):4980–92.
43. Subramanian A, Tamayo P, Mootha VK, Mukherjee S, Ebert BL, Gillette MA, Paulovich A, Pomeroy SL, Golub TR, Lander ES, Mesirov JP. Gene set enrichment analysis: a knowledge-based approach for interpreting genome-wide expression profiles. Proc Natl Acad Sci U S A. 2005;102:15545–50.
44. Tomczak K, Czerwińska P, Wiznerowicz M. The Cancer Genome Atlas (TCGA): an immeasurable source of knowledge. Contemp Oncol (Pozn). 2015;19:A68–77.
45. Goldman MJ, Craft B, Hastie M, Repečka K, McDade F, Kamath A, Banerjee A, Luo Y, Rogers D, Brooks AN, Zhu J, Haussler D. Visualizing and interpreting cancer genomics data via the Xena platform. Nat Biotechnol. 2020;38:675–8.
46. Barrett T, Wilhite SE, Ledoux P, Evangelista C, Kim IF, Tomashevsky M, Marshall KA, Phillippy KH, Sherman PM, Holko M, Yefanov A, Lee H, Zhang N, et al. NCBI GEO: archive for functional genomics data sets–update. Nucleic Acids Res. 2013;41:D991–5.
47. Hugo W, Zaretsky JM, Sun L, Song C, Moreno BH, Hu-Lieskovan S, Berent-Maoz B, Pang J, Chmielowski B, Cherry G, Seja E, Lomeli S, Kong X, et al. Genomic and transcriptomic features of response to Anti-PD-1 therapy in metastatic melanoma. Cell. 2016;165:35–44.
48. Mariathasan S, Turley SJ, Nickles D, Castiglioni A, Yuen K, Wang Y, Kadel EE III, Koeppen H, Astarita JL, Cubas R, Jhunjhunwala S, Banchereau R, Yang Y, et al. TGFβ attenuates tumour response to PD-L1 blockade by contributing to exclusion of T cells. Nature. 2018;554:544–8.
49. Charoentong P, Finotello F, Angelova M, Mayer C, Efremova M, Rieder D, Hackl H, Trajanoski Z. Pan-cancer immunogenomic analyses reveal genotype-immunophenotype relationships and predictors of response to checkpoint blockade. Cell Rep. 2017;18:248–62.
50. Chandrashekar DS, Karthikeyan SK, Korla PK, Patel H, Shovon AR, Athar M, Netto GJ, Qin ZS, Kumar S, Manne U, Creighton CJ, Varambally S. UALCAN: an update to the integrated cancer data analysis platform. Neoplasia. 2022;25:18–27.
51. Tang Z, Kang B, Li C, Chen T, Zhang Z. GEPIA2: an enhanced web server for large-scale expression profiling and interactive analysis. Nucleic Acids Res. 2019;47:W556–60.
52. Sun D, Wang J, Han Y, Dong X, Ge J, Zheng R, Shi X, Wang B, Li Z, Ren P, Sun L, Yan Y, Zhang P, Zhang F, Li T, Wang C. TISCH: a comprehensive web resource enabling interactive single-cell transcriptome visualization of tumor microenvironment. Nucleic Acids Res. 2021;49:D1420–30.
53. Kim J, Yu W, Kovalski K, Ossowski L. Requirement for specific proteases in cancer cell intravasation as revealed by a novel semiquantitative PCR-based assay. Cell. 1998;94:353–62.

Publisher's Note